This is a preprint, the final version is subject to change, of the American Mineralogist (MSA)
Cite as Authors (Year) Title. American Mineralogist, in press.
DOI: https://doi.org/10.2138/am-2020-7013

REVISION II

Partitioning of V and 19 other trace elements between rutile and silicate melt as a function of oxygen fugacity and melt composition: Implications for subduction zones

Megan Holycross[1], Elizabeth Cottrell[1]

[1]National Museum of Natural History, Smithsonian Institution

Abstract

Vanadium is a multivalent element that can speciate as V^{2+}; V^{3+}; V^{4+} and V^{5+} over a range of geologically relevant oxygen fugacities (fO_2). The abundance of V in planetary materials can be exploited as a proxy for fO_2 when its partitioning behavior is known. The mineral rutile (TiO_2) is an important carrier of the high field strength elements Nb and Ta in the solid Earth, but it can also incorporate substantial quantities of vanadium (up to ~2,000 ppm; e.g., Zack et al. 2002). However, little work has been done to systematically investigate how the partitioning of V in rutile-bearing systems changes as a function of both fO_2 and composition. We measured the partitioning of V and 19 other trace elements (Sc, Cr, Y, Zr, Nb, La, Ce, Pr, Nd, Sm, Eu, Gd, Dy, Ho, Er, Yb, Lu, Hf and Ta) between rutile and three silicate melt compositions equilibrated at 1 atmosphere pressure, 1300 °C and fO_2s from two log units below the quartz-fayalite-magnetite oxygen buffer (QFM-2) to air (QFM+6.5). Rutile/melt partition coefficients ($D_V^{rt/melt}$) change dynamically over an eight-log unit range of fO_2 and are greatest at fO_2=QFM-2 in all compositions. Vanadium solubility in rutile declines continuously as fO_2 increases from QFM-2 and approaches unity in air. Trace element partitioning between rutile and melt is also correlated with melt composition, with the greatest values of $D^{rt/melt}$ measured in the most polymerized melt systems containing the least TiO_2. We do not find any circumstances where V becomes

incompatible in rutile. Our results indicate that rutile is a considerable sink for V at terrestrial fO_2s and will contribute to the retention of V in refractory slab residues in subduction zones. In agreement with previous work, we find that $D_{Ta}^{rt/melt} > D_{Nb}^{rt/melt}$ under all conditions investigated, suggesting that rutile fractionation does not lead to low Nb/Ta ratios in Earth's continental crust.

1. Introduction

Oxygen fugacity (fO_2) is a thermodynamic parameter that influences, to a first order, the structure of the planet, the chemistry of rocks and ores, and mass transfer between terrestrial reservoirs (Frost and McCammon 2008). Oxygen fugacity also controls the speciation of multivalent elements in planetary materials and their distribution between phases, which can be used as a proxy for fO_2. Vanadium (V) is a trace element that may have up to four valence states (V^{2+}; V^{3+}; V^{4+} and V^{5+}) in silicate materials (Fig. 1). Vanadium oxygen barometers (oxybarometers) have been experimentally calibrated for a wide variety of mineral-melt systems to investigate how V partitioning shifts as a function of fO_2 (Arató and Audétat 2017; Canil 1997; Canil 2002; Canil and Fedortchouk 2000; 2001; Mallmann and O'Neill 2009; Laubier et al. 2014; Shishkina et al. 2018; Sossi et al. 2018; Toplis and Corgne 2002; Wang et al. 2019)

The partitioning of vanadium between rutile (TiO_2) and other phases has excellent potential to serve as an oxybarometer for metamorphic rocks. Tetravalent vanadium is dominant in silicate melts at oxygen fugacities relevant to the Earth's upper mantle and crust (Borisov 2013; Lanzirotti et al. 2018; Sutton et al. 2005) and has the same valence and an ionic radius similar to Ti^{4+} (0.58 and 0.605 Å in octahedral coordination, respectively; Shannon 1976). Tetravalent vanadium may readily substitute for Ti^{4+} in rutile and the incorporation of "bulk" or total V in rutile should vary as the amount of V^{4+} changes. However, only two previous studies have investigated the partitioning of V between rutile and silicate melt under controlled oxygen

fugacity (Klemme et al. 2005 and Mallmann et al. 2014). The combined data set of Klemme et al. (2005) and Mallmann et al. (2014) show V solubility in rutile is redox-controlled over a 12 log-unit range in fO_2, but scatter in their experimental data suggests a secondary influence on the behavior of vanadium that was not investigated as an experimental variable.

Quantifying the partitioning of trace elements between rutile and melt is also crucial for evaluating the flux of cations through the subduction factory. Rutile is known to concentrate the high field strength elements (HFSE) Nb and Ta in the solid Earth (e.g., Meinhold 2010; Rudnick et al. 2000; Tang et al. 2019; Xiao et al. 2006; Zack et al. 2002). The strong compatibility of these elements in rutile produces complementary liquids depleted in the HFSE during melting or dehydration—a common feature of arc magmas in subduction zones (e.g., Elliott 2003; Gill 1981; Kelemen et al. 2003; Rudnick et al. 2000; Tang et al. 2019; Turner and Langmuir 2015). This observation has motivated an abundance of studies investigating the partitioning of Nb and Ta between rutile and melt (Bromiley and Redfern 2008; Foley et al. 2000; Green 2000; Green and Pearson 1987; Horng and Hess 2000; Jenner et al. 1993; John et al. 2011; Klemme et al. 2005; Mallmann et al. 2014; McCallum and Charette 1978; Ryerson and Watson 1987; Schmidt et al. 2004; Wendlandt 1990; Xiong et al. 2005; Xiong et al. 2011). However, rutile can concentrate vanadium in quantities that rival those of Nb and Ta (up to 2,000 ppm; Barth et al. 2002; Guo et al. 2017; Hermann 2002; Liu et al. 2014; Zack et al. 2002), which suggests that rutile may preferentially retain V as well as the HFSE during slab melting or dehydration. The pioneering study of Shervais (1982) showed the Ti/V ratios of arc basalts are lower than the Ti/V ratios of mid-ocean ridge basalts. We suggest that this tectonic control on Ti and V in volcanic rocks may be in part due to retention of these elements by residual rutile in subduction environments.

This contribution reports experiments to calibrate the partitioning of V and 19 other trace elements between rutile and three silicate melt compositions over an eight and a half log-unit range in oxygen fugacity. Our experiments were executed at ambient pressure in a system where fO_2 can be directly controlled to build intuition for how V behavior correlates with both redox state and melt composition in higher-pressure conditions relevant to rutile growth in nature.

2. Methods

2.1 Experimental

Three systems with a range of melt structures were selected to measure the partitioning of trace elements between rutile and melt as a function of oxygen fugacity and composition. Two synthetic compositions, a dacite and a mid-ocean ridge basalt, were prepared by mixing reagent oxides and silicate mineral powders under ethanol. The third composition was mixed from crushed and powdered natural Lake County obsidian (LCO). Compositional data for all starting materials is listed in Table 1. The three base compositions were subsequently doped with a trace element oxide mix so the final compositions contained ~2,500 ppm V and ~60 ppm each of Sc, Cr, Y, Zr, Nb, La, Ce, Pr, Nd, Sm, Eu, Gd, Dy, Ho, Er, Yb, Lu and Ta. Melts also contained trace amounts of Ni and Hf, likely present as minor contaminants in the silicate mineral powders used in the synthetic mixes.

The pressure, temperature, and compositional conditions for rutile saturation in silicate melts are well-constrained. Rutile solubility is inversely correlated with pressure (P) and melt polymerization and positively correlated with temperature (T) (i.e., TiO_2 is most soluble in depolymerized melts at low P and high T; e.g., Gaetani et al. 2008; Ryerson and Watson 1987; Xiong et al. 2005; Xiong et al. 2009). To avoid any complications from extrapolating rutile

solubility data at high pressure to ambient conditions, we determined the relationship between rutile solubility and the ratio of non-bridging oxygens to tetrahedrally coordinated cations in the melt (NBO/T; Mysen 1983) from previous studies conducted at P=1 atm (see discussion in Section 3.1). Additional TiO_2 was added to powdered mixes to saturate each melt composition in rutile. Powdered rutile (Alfa Aesar; 99.9 % TiO_2) was added to the LCO, dacite and MORB mixes to form bulk compositions containing 11, 17 and 31 wt% TiO_2, respectively.

All experiments were run in a vertical Deltech furnace plumbed with CO and CO_2 gas lines. Experiment fO_2s were monitored using a ZrO_2 sensor referenced to pure O_2. The hot spot of the furnace was mapped using the technique of Walker et al. (1988) and the thermocouple temperature was calibrated relative to the melting point of Au at one atmosphere.

Experiment starting materials were blended with liquid polyvinyl alcohol and hung from Pt loops. All Pt loops were pre-equilibrated with the starting material to mitigate loss of Fe from the melt to the loop during partitioning experiments (Grove 1982). Pre-equilibration runs were held at 1300 °C and the targeted fO_2 for 24 hours. Loops were cleaned in HF and reloaded with starting material for partitioning experiments. Rutile/melt partitioning experiments were fused at 1500 °C for ~1 h to create a homogeneous melt and cooled at 6 °C/h for equilibratation at 1300 °C. Experiment conditions are recorded in Table 2. All runs were terminated by drop-quenching the experiments in water inside the controlled-atmosphere furnace. Completed experiments were mounted in epoxy, exposed and polished for analysis.

2.2 Analytical

We confirmed the presence of rutile in our run products with Raman spectroscopy. Raman spectra were collected on all experiments using a Horiba LabRAM HR Evolution

confocal microscope equipped with Synapse detector at the National Museum of Natural History (NMNH), Smithsonian Institution. Spectra were collected at the 532 nm wavelength using a 600 μm grating and a 5 μm focused spot size for all experiments except the LCOTi series, where a 2.5 μm spot was used. Collected spectra were reduced in the LabSpec6 software and compared to entries in the RRUFF online database (Downs 2006) to confirm the presence of rutile in our experiments. Examples of collected Raman spectra are reported in the Supplemental Material.

The major and minor element compositions of all experiments were determined using the JEOL 8530F Hyperprobe at NMNH. A correction was used to account for the overlap of the Ti K_β peak with the V K_α peak on the LIF crystal (Snetsinger 1964). A Ti-Cr-V metal alloy (NIST SRM-649) was used as a secondary standard during EPMA analysis. Repeated analyses of pure Ti metal using our correction returned values of "0" for vanadium. Experimental glasses were measured at an accelerating voltage of 15 kV and 10 nA current using a defocused 20 μm spot to reduce Na loss. Experimental rutile was measured at 15 kV and 20 nA current using a 1 μm spot size. Counting times were 60 s for V and 20 s for all other elements. Concentrations of V in all experimental materials were well above the EPMA detection limit (~100 ppm) for our analytical routine. Multiple analyses on single grains and rim-to-rim traverses showed no signs of crystal zoning in our experiments (reported in the Supplemental Material).

The trace element compositions of three experiments were determined via laser ablation ICP-MS in the Corman Center for Mass Spectroscopy at Rensselaer Polytechnic Institute. The RPI LA-ICP-MS consists of a Photon Machines Analyte 193 nm ultra-short pulse excimer workstation coupled to a Bruker 820 quadrupole ICP-MS. We applied a laser fluence of 7.19 J/cm^2 and 6 Hz rep rate. For all analyses, the sample was ablated for 30 s, followed by 30 s where the shutter was closed to measure the background. All experimental glasses were analyzed

using a 40 μm laser spot. Rutile was analyzed with a 40 or 20 μm laser spot, depending on rutile grain size. NIST612 glass (Pearce et al. 1997) was used as the standard for glass analyses. USGS-GS1D glass was used as the standard for rutile analyses and as a secondary standard for analyses of experimental glasses. Trail et al. (2018) demonstrates matrix-matched mineral standards are not necessary for laser spot sizes ≥20 μm. LA-ICP-MS data were reduced using the Iolite software package for Igor Pro (Paton et al. 2011) with ^{29}Si and ^{49}Ti as the internal standards for glasses and rutile, respectively, in the trace element data reduction scheme. We monitored major element ratios (i.e., ^{27}Al:^{49}Ti) to filter out any glass signal in our rutile spectra. The small size of rutile in most experiments precluded LA-ICP-MS measurements. Complete chemical data for all experiments are collated in the Supplemental Material.

3. Results

Sixteen partitioning experiments saturated in rutile. One experiment conducted in air saturated in an armacolite (Ti-Mg-Fe-Al) solid solution (Anderson et al. 1970) in addition to rutile (chemical data may be found in Supplemental Material). Basaltic melt experiments crystallized large, subhedral rutile grains while more polymerized melts (DacTi and LCOTi experiments) promoted the growth of euhedral, acicular rutile crystals (Fig. 2). Rutile needles formed clusters and were oriented similarly in the more polymerized melt compositions (Figures 2b and 2c), indicating Ti may have structural influence as a nucleating agent for crystal growth in silicate melts (Guignard et al. 2010). Rutile saturation is strongly correlated to the degree of melt polymerization (Fig. 3).

Rutile/melt partition coefficients were calculated from chemical data according to the equation

This is a preprint, the final version is subject to change, of the American Mineralogist (MSA)
Cite as Authors (Year) Title. American Mineralogist, in press.
DOI: https://doi.org/10.2138/am-2020-7013

158 $$D^{rt/melt} = \frac{concentration\ in\ rutile}{concentration\ in\ melt} \quad (1)$$

159 Reported standard deviations were calculated from

160 $$\sigma = \sqrt{{SD_{melt}}^2 + {SD_{rt}}^2} \quad (2)$$

161 Rutile/melt partition coefficients for V are listed in Table 2. All other trace element partition
162 coefficients are presented in Table 3.

163 Element diffusion in silicate melts is dependent on melt polymerization. The experiments
164 of Holycross and Watson (2016; 2018) show vanadium diffusion in dry basaltic melts at 1300
165 ºC is almost twice as fast as V diffusion in hydrous rhyolitic melts at the same temperature (no
166 diffusion data has been published for V in dry rhyolitic melts, but it is likely slower than V
167 diffusion in hydrous rhyolitic melts). We employed the same experimental cooling rate for all
168 melt compositions. This raises the possibility that rutile in our most polymerized melt
169 compositions did not crystallize in equilibrium with the bulk melt and may instead sample a melt
170 region surrounding the crystal that has not diffusively equilibrated (see contributions by
171 Albarede and Bottinga 1972; Holycross and Watson 2016; 2018; Sossi and O'Neill 2016; and
172 Watson and Müller 2009 among others for discussion on how diffusive boundary layers in the
173 melt impact the disequilibrium incorporation of cations in rapidly growing minerals). However,
174 EPMA traverses across rutile/melt interfaces and rutile grains from all compositions (reported in
175 the Supplemental Material) confirm V concentrations in rutile are homogeneous from rim-to-rim,
176 as are melt regions surrounding the crystal interface. In addition, two experiments of different
177 duration (231 and 40 hours) in the DacTi system at QFM+1 produce the same values of $D_V^{rt/melt}$
178 within 2σ, indicating our experiment durations were sufficient to attain equilibrium.

This is a preprint, the final version is subject to change, of the American Mineralogist (MSA)
Cite as Authors (Year) Title. American Mineralogist, in press.
DOI: https://doi.org/10.2138/am-2020-7013

4. Discussion

4.1 Rutile defect equilibria and relationship to oxygen fugacity

Rutile is a non-stoichiometric phase (TiO_{2-x}, where x=0-0.02) with semiconducting and photocatalytic properties that are closely related to its concentration of point defects (e.g., Bak et al. 2012, Kofstad 1972, Nowotny et al. 2008). A decrease in oxygen fugacity results in the formation of two main "donor" point defects in rutile: oxygen vacancies (dominant; $v_O^{\cdot\cdot}$ in Kröger-Vink notation) and interstitial titanium sites (minor; $Ti_i^{\cdot\cdot\cdot\cdot}$ and $Ti_i^{\cdot\cdot\cdot}$ for Ti^{4+} and Ti^{3+} interstitials, respectively) (Kofstad 1972). Formation of point defects increases the population of free electrons; thus as fO_2 decreases, the rutile structure can accommodate a greater array of ions with different valence states and electronegativities to charge balance. According to the defect model of Bak et al. (2012), both $v_O^{\cdot\cdot}$ and $Ti_i^{\cdot\cdot\cdot\cdot}$ are constant in rutile at our experimental conditions (absolute logfO_2=-9.21 to -0.6 bar at 1300 ºC), which suggests the main substitution mechanism for V in our experiments is exchange of V^{4+} for Ti^{4+}. Our system is not reducing enough to stabilize any significant amount of trivalent titanium (e.g., Borisov 2012; Leitzke et al. 2018) and $Ti_i^{\cdot\cdot\cdot}$ is orders of magnitude less than $v_O^{\cdot\cdot}$ and $Ti_i^{\cdot\cdot\cdot\cdot}$. However, $Ti_i^{\cdot\cdot\cdot}$ increases substantially with decreasing fO_2 and we anticipate that the exchange of V^{3+} with Ti^{3+} sites may become important for the incorporation of V in TiO_2 under more reducing conditions.

We note that the model of Bak et al. (2012) describes the defect structure of rutile crystals equilibrated with gas atmospheres, while our experimental rutile equilibrated with TiO_2-bearing silicate melt. Additional defects in our experimental rutile may result from the substitution of major cations like Si, Fe or Al (e.g., Cherniak and Watson 2019; Hoff 2019) or may be correlated with the activity of TiO_2 in the melt.

This is a preprint, the final version is subject to change, of the American Mineralogist (MSA)
Cite as Authors (Year) Title. American Mineralogist, in press.
DOI: https://doi.org/10.2138/am-2020-7013

4.2 Vanadium partitioning between rutile and melt

4.2.1 Redox dependence of partitioning

The partitioning of "bulk" vanadium between rutile and melt is driven by the shift in V valence state over the eight and a half log-unit range in fO_2 investigated here (Figure 4). Divalent vanadium is negligible at fO_2=QFM-2 and above (Sutton et al., 2005) and we only consider the oxidation reactions

$$V^{3+}O_{1.5} + {}^{1}/_{2}\,O_2 = V^{5+}O_{2.5} \quad (3a)$$

$$V^{4+}O_2 + {}^{1}/_{4}\,O_2 = V^{5+}O_{2.5} \quad (3b)$$

in our experimental system. The equilibrium constants (K) for redox reactions 3a and 3b are given by

$$K_{3a} = \frac{V^{5+}O_{2.5}}{(V^{3+}O_{1.5})(fO_2)^{1/2}} \quad (4a)$$

$$K_{3b} = \frac{V^{5+}O_{2.5}}{(V^{4+}O_2)(fO_2)^{1/4}} \quad (4b)$$

The thermodynamic treatment of Mallmann and O'Neill (2009) calculates the bulk partition coefficient, $D_V^{min/melt}$, from the partition coefficients for individual V species, $D_{V^{3+}}^{min/melt}$, $D_{V^{4+}}^{min/melt}$ and $D_{V^{5+}}^{min/melt}$ and the equilibrium constants K_{3a} and K_{3b}. We used the parameterization of Mallmann and O'Neill (2009) to determine the relationship between $D_V^{rt/melt}$ and oxygen fugacity for each melt composition from the equation

$$D_V^{rt/melt} = \frac{\left(D_{V^{3+}}^{rt/melt}\cdot(K_{3a})^{-1}\cdot(fO_2)^{-1/2}\right)+\left(D_{V^{4+}}^{rt/melt}\cdot(K_{3b})^{-1}\cdot(fO_2)^{-1/4}\right)+D_{V^{5+}}^{rt/melt}}{\left((K_{3a})^{-1}\cdot(fO_2)^{-1/2}\right)+\left((K_{3b})^{-1}\cdot(fO_2)^{-1/4}\right)+1} \quad (5)$$

Mallmann and O'Neill (2009) note that values of *K* are less sensitive to melt composition than values of *D*. We apply the equilibrium constants (K_{3a}=3.03 x 10^{-5} and K_{3b}=3.09 x 10^{-3}) of Mallmann and O'Neill (2009) to model redox reactions in our rutile-melt systems (note that other studies have found different *K*s for magnetite/melt partitioning of V, e.g., Sossi et al. 2018; Toplis and Corgne 2002). More details on this modeling approach may be found in Mallmann and O'Neill (2009). Rutile/melt partition coefficients for each valence state of V are reported in our Supplemental Material.

Each melt system produces distinct partition coefficients for V^{3+}, V^{4+} and V^{5+} and values of $D_{V^{4+}}^{rt/melt} > D_{V^{3+}}^{rt/melt} > D_{V^{5+}}^{rt/melt}$ in all compositions (Supplemental Material). Tetravalent vanadium is most abundant in our system at fO_2s near QFM-2 (Sutton et al. 2005), has the same valence and an ionic radius very similar to Ti^{4+} in octahedral coordination (Shannon, 1976). Rutile/melt partition coefficients for bulk V are greatest when V^{4+} is the dominant species—$D_V^{rt/melt}$ peaks at QFM-2 in all melt compositions. $D_V^{rt/melt}$ decreases continuously as fO_2 increases and V^{5+} becomes prevalent. Rutile/melt partition coefficients approach unity near fO_2=QFM+6.5, but V never becomes incompatible in rutile in our experiments.

It is unclear from our experiments how V^{3+} behaves in the rutile-melt system. Mismatch between the ionic radii of V^{3+} and Ti^{4+} (Shannon, 1976) indicates $D_V^{rt/melt}$ should decrease as V^{3+} becomes abundant at fO_2<QFM-2. However, the solubility of V^{3+} may be enhanced by coupled substitution with pentavalent ions like Nb and Ta, which are highly compatible in rutile (see Section 4.3). Trivalent vanadium is also expected to exchange with Ti^{3+} in systems under very reducing conditions (Bak et al. 2012; Borisov 2013; Papike et al. 2016). Substitution mechanisms for V^{3+}, while of crystal-chemical interest, are less important for terrestrial systems

where V^{4+} and V^{5+} are dominant and further consideration is beyond the scope of this contribution.

4.2.2 Compositional dependence of partitioning

Rutile/melt partition coefficients for V vary systematically between the three melt compositions at a given fO_2 (Figure 6). Partition coefficients obtained for the MORB system are the lowest at all fO_2s investigated and are close to an order of magnitude less than $D_V^{rt/melt}$ in LCO at $fO_2 \leq$QFM. The dacite system produced intermediate values of $D_V^{rt/melt}$ at all fO_2 conditions. The behavior of V at a given fO_2 is clearly dependent on melt composition and is influenced by both melt polymerization (i.e., NBO/T) and the TiO_2 content of the melt.

Early experimental work by Watson (1976) and Ryerson and Hess (1978) predicted mineral/melt partition coefficients for elements with high charge densities (i.e., the HFSE) will increase with increasing polymerization of the melt. Subsequent studies by Green and Pearson (1987), Wendlandt (1990), Horng and Hess (2000), Green (2000), Schmidt et al. (2004), Klemme et al. (2005), Xiong et al. (2005), Xiong et al. (2011), and this contribution, show strong correlations between rutile/melt partitioning of the HFSE and melt polymerization. Our new experiments demonstrate vanadium behaves similarly to the HFSE: $D_V^{rt/melt}$ increases as NBO/T decreases in the three melt compositions (Fig. 6a).

Vanadium partitioning between rutile and melt may also be correlated with the coordination of Ti in the melt. The role of titanium in silicate melt structures is concentration-dependent, and it's in both the numerator and denominator of the "NBO/T" ratio (Mysen 1983). X-ray absorption near edge structure (XANES) spectroscopy of silicate glasses shows the relationship between Ti coordination and melt composition , as well as pressure and temperature,

is highly complex (e.g., Farges et al. 1996; Farges and Gordon 1997; Greegor et al. 1983; Romano et al. 2000). Titanium may be coordinated as $^{[5]}$Ti and $^{[6]}$Ti in depolymerized melts but becomes coordinated as $^{[4]}$Ti as NBO/T decreases (Dingwell et al. 1992; Farges et al. 1996; Farges and Gordon 1997). Highly coordinated Ti can form Ti-O-Ti rutile-structured complexes in depolymerized melts, while $^{[4]}$Ti is predicted to form Ti-O-Si linkages in more polymerized compositions (Farges et al. 1996). Greegor et al. (1983) observed six-fold coordinated Ti in silicate glasses only when they contained >7 wt% TiO_2; fourteen of our sixteen experimental glasses contain >7 wt% TiO_2 (Table 2).

Octahedrally-coordinated Ti structures in the melt may form rutile-like complexes that bind rutile-compatible cations, leading to lower rutile/melt partition coefficients for these elements in Ti-rich melt systems. This effect likely contributed to the compositional trends in our rutile/melt partitioning data. It is well-established that highly polymerized melts require less bulk TiO_2 to saturate in rutile (e.g., Fig. 3 and Dickinson and Hess 1985; Gaetani et al. 2008; Ryerson and Watson 1987; Schmidt et al. 2004; Xiong et al. 2005; Xiong et al. 2009). Our basaltic system contained more TiO_2 to saturate in rutile than the dacitic system, which contained more TiO_2 than the rhyolitic system (Fig. 6b). Depolymerized melts contain more, and more highly coordinated, TiO_2 in equilibrium with rutile. Consequently, $D_V^{rt/melt}$ at a given fO_2 can be expressed as a function of both NBO/T and melt TiO_2 content (Fig. 6). The relationship between rutile solubility and melt polymerization, in addition to the influence of melt TiO_2 on polymerization itself (Mysen 1983) dictates that these parameters cannot be changed independently in our experimental series. No published work has systematically investigated the relationship between fO_2, $D_V^{rt/melt}$ and composition in higher pressure systems that saturate in rutile at lower TiO_2 concentrations.

Previous studies by Xirouchakis et al. (2001), Schmidt et al. (2004), Dygert et al. (2014) and Leitzke et al. (2016) have also noted that *D* values for other mineral/melt systems are inversely correlated with melt TiO_2 content.

4.2.3 Comparison to other studies

Klemme et al. (2005) and Mallmann et al. (2014) have also examined the partitioning of V between rutile and silicate melt as a function of oxygen fugacity. Those two studies were conducted at the same conditions (P=1 atm, T=1250-1300 °C), used identical melt compositions, and yielded similar results (Figure 5). A notable exception is that some of the experiments of Klemme et al. (2005) suggest V is more compatible in rutile under oxidizing conditions than the experiments of Mallmann et al. (2014). Our new data agree with their previous work at $\log fO_2$<QFM+1 but deviate significantly at more oxidizing conditions (Figure 5). This discrepancy is most likely due to the difference in the melt compositions used here and those of Klemme et al. (2005) and Mallmann et al. (2014), which contained more TiO_2 and were less polymerized (see Section 4.2.2). Mallmann et al. (2014) reported a progressive increase in $D_V^{rt/melt}$ even as fO_2 was reduced to QFM-5. This behavior may be expected as fO_2 decreases due to both an increased number of point defects in rutile (Bak et al. 2012) and increased exchange of V^{3+} with Ti^{3+} species formed at reducing conditions (Borisov 2012). However, Mallmann et al. (2014) interpreted this trend to reflect the enhanced stabilization of V^{4+} to lower fO_2 than previously expected and did not find any evidence for the presence of V^{3+} in their experiments. In contrast to Klemme et al. (2005) and Mallmann et al. (2014), we do not find any conditions where V becomes incompatible in rutile (Fig. 5).

4.2.4 What controls V incorporation in terrestrial rutile?

In this experimental series, we varied fO_2 and melt composition. In these 1-atmosphere experiments, by necessity, the concentration of TiO_2 greatly exceeds what we expect in nature. Further, variation in TiO_2 directly influences the melt's NBO/T ratio, such that TiO_2 and NBO/T cannot be varied independently (they co-vary with $R^2 = 0.95$). Multiple regressions of fO_2, NBO/T and TiO_2 therefore results in multicollinearity. Melt TiO_2 concentration and NBO/T do not provide independent information, and one must be dropped from the regression. As expected with multicollinearity, the result of the regression is the same whether cast in terms of NBO/T or TiO2 – each variable accounts for ~ 30% of the variance in $D_V^{rt/melt}$. Because $D_V^{rt/melt}$ is likely to correlate with any component that alters NBO/T, and because TiO_2 does not vary widely in terrestrial melts, we choose to cast the dependent variable in terms of fO_2 and NBO/T (for n=16 experiments, $R^2 = 0.67$, and p-value =0.002 for both NBO/T and fO_2).

In sum, the partitioning of V between rutile and melt in our experiments is controlled equally by fO_2 and melt composition, over the range of fO_2 and melt composition investigated. It is uncertain how these influences are borne out in terrestrial environments because our experiments employed unnatural melt compositions. Rutile saturation is dependent on melt polymerization (investigated here) as well as pressure and temperature. Terrestrial magmas contain a limited amount of TiO_2 (often 0.5-3 wt% with a maximum of 5.5 wt%; e.g., Arndt et al. 1995; Dasgupta et al. 2010; Gale et al. 2013; Turner and Langmuir 2015) and do not precipitate rutile unless they are fairly polymerized (e.g., Ryerson and Watson 1987; Xiong et al. 2009). In contrast, the available data suggest that rutile saturation is not directly limited by fO_2, and can occur over a wide extent of Earth-relevant redox conditions (e.g., this contribution as well as Guo et al. 2017; Klemme et al. 2005; Liu et al. 2014; Mallmann et al. 2014).

Terrestrial rutile equilibrates with silicate melts over a narrow range of NBO/T and TiO_2 but a potentially large and uncertain range of fO_2. It's noteworthy that our most polymerized experimental system with the least TiO_2 returned the highest partition coefficients, and also produced the greatest dynamic range of $D_V^{rt/melt}$—i.e., $D_V^{rt/melt}$ was most sensitive to changes in redox in this melt composition. We suggest that in natural systems with reasonable melt compositions, fO_2 will be the dominant free parameter controlling the incorporation of V in natural rutile.

4.2.5 Anticipated effects of pressure and temperature on vanadium partitioning between rutile and melt

Two previous studies have measured the partitioning of V between rutile and melt at higher pressures and lower temperatures but have not controlled or monitored fO_2. However, we can use their results to make qualitative predictions about the behavior of V-in-rutile under *P* and *T* conditions more relevant to natural rutile saturation scenarios.

Foley et al. (2000) reported the results of three experiments to measure the partitioning of trace elements between rutile and tonalite melt at *P*=18-25 kbar and *T*=900-1100 °C. They estimated their experimental assembly imposed fO_2s close to the Fe-FeO buffer (~QFM-5 at this *P* and *T* range). Foley et al. (2000) produced $D_V^{rt/melt}$ = 46.5-124. Xiong et al. (2005) ran eclogite melting experiments to measure trace element partitioning between rutile and hydrous silicic melt at *P*=10-25 kbar and *T*=925-1075 °C. They estimated their experimental fO_2s to be between the Fe_3O_4-FeO and Ni-NiO and buffers (~QFM+0.5 to ~QFM-2.5). Xiong et al. (2005) found $D_V^{rt/melt}$ = 40-141, with no clear trend between $D_V^{rt/melt}$, *T* or *P* in their experiments.

Values of $D_V^{rt/melt}$ measured by Foley et al. (2000) and Xiong et al. (2005) are 2 to 6 times greater than any value of $D_V^{rt/melt}$ measured in this study (22, at QFM-2 in LCOTi) and near 1.5 orders of magnitude greater than all values of $D_V^{rt/melt}$ returned in the MORBTi system (Table 2). Clearly, increasing pressure and/or decreasing temperature substantially increases the compatibility of V in rutile. Foley et al. (2000) and Xiong et al. (2005) also measured $D_{Nb}^{rt/melt}$ and $D_{Ta}^{rt/melt}$ in the same experiments as $D_V^{rt/melt}$; in runs that produced the highest values of $D_V^{rt/melt}$ (≥100), vanadium compatibility in rutile is similar to the HFSE ($D^{rt/melt}$ also ~100). Considering our new data in concert with the previous work of Foley et al. (2000) and Xiong et al. (2005), we predict rutile may be a substantial carrier of V in addition to the HFSE in subduction zone environments, especially at fO_2s at or below the QFM buffer.

4.3 Other trace elements

Three of our experiments produced rutile large enough for laser ablation analysis. Our trace element partition coefficients (Table 3) agree qualitatively with previous studies conducted under similar conditions (Klemme et al. 2005; Mallmann et al. 2014). Increasing melt polymerization drives an increase in the compatibility of all trace elements in rutile (Fig. 8). All rare earth elements are broadly incompatible in rutile. Rutile/melt partitioning of multivalent Cr and Fe increases as fO_2 increases from QFM-2 to QFM-1 in the MORBTi system, which may indicate a coupled substitution mechanism for Fe^{3+} and Cr^{3+} with Nb^{5+} or Ta^{5+}.

We find that niobium and tantalum are extremely compatible in rutile ($D^{rt/melt}$=50 to 230). Variations in the partitioning of Nb and Ta between rutile and melt may be linked to changes in either melt polymerization or melt TiO_2 content (Section 4.2.2). In agreement with previous work, we find that $D_{Ta}^{rt/melt}>D_{Nb}^{rt/melt}$ under all conditions investigated (Bromiley and Redfern 2008; Foley et al. 2000; Green 2000; Green and Pearson 1987; Horng and Hess 2000; Jenner et

al. 1993; John et al. 2011; Klemme et al. 2005; Mallmann et al., 2014; Schmidt 2004; Wendlandt 1990; Xiong et al. 2005; Xiong et al. 2011). However, we note that analyses of Ta in our experimental rutile exhibit a slightly higher standard deviation than our Nb values (~11% S.D. compared to ~3% S.D., respectively; see Supplemental Material). This may be due to either poorer counting statistics for the less abundant Ta, or the due to the slower diffusivity of Ta relative to Nb in rutile (Dohmen et al., 2018; Marschall et al. 2013).

5. Implications

Shervais (1982) found arc basalts have lower Ti/V ratios than MORB (Ti/V=10-20 and Ti/V=20-50, respectively, after filtering for magnetite fractionation) but asserts the lower Ti/V of arcs cannot be due to retention of Ti-rich phases in refractory residues unless the Ti-rich phase also strongly retains vanadium. Our new data show that the Ti-phase rutile, which commonly forms in MORB subducted to eclogite facies, strongly retains vanadium and its compatibility in rutile is dependent on the oxygen fugacity of the system. This raises the possibility the Ti/V signature of arc magmas may be in part inherited from a low Ti/V component that has been transferred from a rutile-bearing slab and subsequently mixed with the overlying arc.

Dynamic and thermochemical models indicate that slab-surface temperatures reach or exceed the hydrous basalt + sediment solidus for roughly half of the world's subduction zones (e.g., Cooper et al. 2012; Hermann and Rubatto 2009; Plank et al. 2009; Syracuse et al. 2010; van Keken et al. 2002); recent work by Sisson and Kelemen (2018) suggests eclogite partial melts constitute 1/10 to 1/3 of the final parental arc magmas. Eclogite melting is thus not only a common phenomenon during subduction but also plays a critical role in controlling the flux of elements from the slab to the overlying arc. Here, we model partitioning of Ti and V during eclogite melting as a function of fO_2 and phase assemblage (garnet, clinopyroxene ± rutile) to

397 determine the impact of residual rutile on the Ti/V ratios of slab melts and their potential
398 contribution to parental arc magmas.

399 We have produced rutile/melt partition coefficients for V over varying fO_2. Several
400 previous studies have measured the partitioning of V between garnet/melt (Canil 2001;
401 Mallmann and O'Neill 2009 following Mallmann et al. 2007; Righter et al. 2011) and
402 clinopyroxene/melt (Canil 2001; Canil and Fedortchouk 2000; Laubier et al. 2014; Mallmann
403 and O'Neill 2009; Wang et al., 2019) under controlled oxygen fugacity. At present there are no
404 reported data sets examining partitioning of V between these phases as function of fO_2 at
405 pressures, temperatures and compositions relevant to slab melting. This necessitates we model V
406 partitioning in our system using available coefficients assuming fO_2, rather than P, T or x, is the
407 most important variable controlling V behavior. We modeled partitioning of V between rutile
408 and slab melts using $D_V^{rt/melt}$ for our LCOTi system at one atm pressure and 1300 ºC—conditions
409 that are plainly outside the realm of possibility for natural eclogite melting scenarios. However,
410 $D_V^{rt/melt}$ may increase significantly at higher P and lower T ($D_V^{rt/melt} \geq 40$ and can exceed 100; see
411 discussion in Section 4.2.5), thus our partition coefficients are realistically minimums for
412 modeling V incorporation in rutile during slab melting. We used $D_V^{cpx/melt}$ from Mallmann and
413 O'Neill (2009) measured at 1300 ºC and 1 atm pressure. Comparison of the studies by Mallmann
414 and O'Neill (2007) and Mallmann and O'Neill (2009) indicate $D_V^{cpx/melt}$ at 1300 ºC and 1 atm
415 overlaps with $D_V^{grt/melt}$ at 3 GPa and 1400-1450 ºC at the same fO_2, and we make the simplifying
416 assumption that $D_V^{grt/melt} = D_V^{cpx/melt}$ in our model. The experiments of Mallmann and O'Neill
417 2007 and 2009 both used mafic melt compositions, but again, it is currently unknown how V
418 partitions between clinopyroxene, garnet and more evolved melt compositions under varying
419 fO_2.

We calculated partitioning of Ti between rutile, clinopyroxene, garnet and melt using the data of Klemme et al. (2002) and Xiong et al. (2009). Partitioning of Ti is constant over changing fO_2. We stress that, although the partition coefficients we input in our model have been measured at temperatures that are significantly hotter than the conditions of eclogite melting on the slab geotherm (solidus at 700-800 ºC, e.g., Sisson and Kelemen 2018), we expect the compatibility of V in all eclogitic minerals to increase down-temperature due to the increased free energy of fusion at lower *T* (Blundy and Wood 2003). Rutile saturation is dependent on temperature; evolved melts at lower temperatures contain less TiO_2 because it precipitates out as rutile (e.g., Klimm et al. 2008; Ryerson and Watson 1987; Xiong et al. 2005). Thus, the compatibilities of V and Ti in eclogite melts may extrapolate down-temperature in a similar way. Even though the conditions of our model are offset from the conditions of slab melting in nature, our data provide first-order results and context for future experiments conducted at high *P*, lower *T* and controlled fO_2. More information about our model can be found in the Supplementary Material.

Figure 8 shows the V content (8a) and Ti/V ratios (8b) of eclogite slab melts at 5% batch melting as a function of fO_2 and mineral assemblage. The three modeled eclogite mineral assemblages contain equal amounts of garnet and clinopyroxene and are either rutile-free or contain 1 or 2% rutile. Rutile is an accessory mineral and its modal percentage in exhumed slabs globally may be closer to 1% (e.g., Hills and Haggerty 1989). However, many subduction-related UHP terranes contain up to 2-4 vol% rutile (e.g., Liou et al., 1998; Kylander-Clark et al. 2008) and eclogites often contain relict rutile that has broken down to ilmenite, titanite or other phases during alteration or exhumation (e.g., Meinhold 2010; Xiao et al., 1998; Zack et al. 2002; Zack and Kooijman 2017 and references therein), which indicates the original proportion of rutile in the rock was possibly greater at the time of prograde eclogite facies metamorphism.

443 The average concentrations of both Ti and V individually, as well as Ti/V ratios, are
444 lower in arcs than in MORB, but the relative decrease in Ti (~50%) is much greater than the
445 decrease in V (~10%) between MORB and arcs (e.g., compare arc magmas reported in Turner
446 and Langmuir 2015 with MORB from Gale et al. 2013 for compositions with the same MgO).
447 Figure 8a shows the addition of 1-2% rutile to the slab residue can deplete V in slab melts by up
448 to 20% at fO_2s where V is most compatible in rutile. This modest effect is likely to be more
449 pronounced at higher pressures and lower temperatures, where previous experimental data
450 suggest $D_V^{rt/melt}$ can reach over 100 (Section 2.5.2). Titanium is incompatible in clinopyroxene
451 and garnet—subsequent additions of 1% rutile to our model assemblage decreases the Ti content
452 of the complementary melt from ~3 wt% to 0.78 wt% to 0.44 wt% (Supplementary Material).

453 At a specified mineral assemblage and melt fraction, the Ti content of the slab melt is
454 constant while the V content changes as a function of fO_2. Increasing quantities of rutile in the
455 slab residue drives an offset in the Ti/V of melts of each assemblage, but the slope of the line is
456 driven by the decreasing compatibility of V in the mineral residue as fO_2 increases. If slab melts
457 do in fact contribute a Ti/V component to the overlying arc that is less than MORB, this
458 component may only be produced by melting of refractory slab residues containing >1 wt%
459 rutile at $fO_2 \geq$QFM. In all other modeled scenarios, the slab melt would contribute a component
460 with much greater Ti/V than MORB, which would require a considerable decrease of Ti/V
461 through another process at convergent margins.

462 Rutile influences the concentration of both Ti and V in eclogite melts and the presence of
463 rutile in slab residues may in part explain the lower ratio of Ti/V in arc rocks observed by
464 Shervais (1982). The high solubility of V in rutile may also impact trace element ratios like V/Sc
465 (Aulbach and Stagno 2016; Lee et al. 2005; Stolper and Bucholz 2019) and V/Yb (Laubier et al.

2014) that have been used as proxies for fO_2 in subduction zone settings, particularly if the arc crust is thick enough to stabilize rutile-bearing "arclogites" at its base (e.g., Ducea et al. 2015; Lee et al. 2006; Rodriguez-Vargas et al. 2005; Tang et al. 2019).

Our experiments indicate rutile is a considerable sink for vanadium in the solid Earth. Vanadium is most soluble in rutile at fO_2s at or below QFM and in high-SiO_2 systems, but we emphasize that the partitioning of V between rutile and melt is greater than unity at all fO_2s investigated. This suggests rutile will contribute to the retention of V in refractory residues during eclogite melting under all but the most oxidizing conditions, where it becomes neutral. The strong compatibility of V in rutile and the dynamic variation of $D_V^{rt/melt}$ as function of fO_2 suggests a rutile-based V-oxybarometer may be robust to even small changes in system redox state.

In agreement with previous work, we find that $D_{Ta}^{rt/melt} > D_{Nb}^{rt/melt}$ under all conditions investigated (Bromiley and Redfern 2008; Foley et al. 2000; Green 2000; Green and Pearson 1987; Horng and Hess 2000; Jenner et al. 1993; John et al. 2011; Klemme et al. 2005; Mallmann et al., 2014; Schmidt 2004; Wendlandt 1990; Xiong et al. 2005; Xiong et al. 2011). Current evidence indicates that rutile fractionation does not lead to low Nb/Ta ratios in Earth's continental crust, as was recently suggested by Tang et al. (2019). However, confirmation under the colder, high-pressure, conditions relevant to arcs awaits further experimental investigation.

Acknowledgements

We thank T. Gooding for his assistance with sample preparation and lab maintenance, R. Wardell for help on the Raman and T. Rose for his oversight of the analytical laboratories. Conversations with M. Ackerson helped shape our discussion of TiO_2. We are grateful for

editorial handling by K. Kiseeva and thorough reviews by P. Sossi, R. Arató and anonymous reviewer, which improved the quality of this manuscript. This study was made possible by a Smithsonian Peter Buck Fellowship to M.H. and a gift from the Lyda Hill Foundation to E.C.

References

Albarede, F., and Bottinga, Y. (1972) Kinetic disequilibrium in trace element partitioning between phenocrysts and host lava. Geochimica et Cosmochimica Acta 36, 141-156.

Anderson, A.T., Boyd, F.R., Bunch, T.E., Cameron, E.N., El Goresy, A., Finger, L.W., Haggerty, S.E., James, O.B., Keil, K., Prinz, M., and Ramdohr, P. (1970) Armalcolite: a new mineral from the Apollo 11 samples. Geochimica et Cosmochimica Acta Supplement, 1, 55.

Arató, R., and Audétat, A. (2017) Experimental calibration of a new oxybarometer for silicic magmas based on vanadium partitioning between magnetite and silicate melt. Geochimica et Cosmochimica Acta, 209, 284-295.

Arndt, N., Lehnert, K., and Vasilev, Y. (1995) Meimechites—highly magnesian lithosphere contaminated alkalkine magmas from deep subcontinental mantle. Lithos, 34, 41-59.

Aulbach, S., and Stagno, V. (2016) Evidence for a reducing Archean ambient mantle and its effects on the carbon cycle. Geology, 44, 751-754.

Bak, T, Bogdanoff, P., Fiechter, S., and Nowotny, J. (2012) Defect engineering of titanium dioxide: full defect disorder. Advanced Applied Ceramics, 111, 62-71.

Barth, M.G., Rudnick, R.L., Horn, I., McDonough, W.F., Spicuzza, M.J., Valley, J.W., and Haggerty, S.E. (2001) Geochemistry of xenolithic eclogites from West Africa, Part I: A link between low MgO eclogites and Archean crust formation. Geochimica et Cosmochimica Acta, 65, 1499-1527.

Borisov, A.A. (2012) The Ti^{4+}/Ti^{3+} ratio of magmatic melts: application to the problem of the reduction of lunar basalts. Petrology, 20, 391-398.

Borisov, A.A. (2013) Mutual interaction of redox pairs in silicate melts: $V^{5+}/V^{4+}/V^{3+}/V^{2+}$ tetrad and other equilibria. Petrology, 21, 305-315.

Bromiley, G.D., and Redfern, S.A.T. (2007) The role of TiO_2 phases during melting of subduction-modified crust: implications for deep mantle melting. Earth and Planetary Science Letters, 267, 301-308.

Canil, D. (1997) Vanadium partitioning and the oxidation state of Archean komatiite magmas. Nature, 389, 842-845. Canil, D. (2002) Vanadium in peridotites, mantle redox and tectonic environments: Archean to present. Earth and Planetary Science Letters 195, 75-90.

Canil, D., and Fedortchouk, Y. (2000) Clinopyroxene-liquid partitioning for vanadium and the oxygen fugacity during formation of cratonic and oceanic lithosphere. Journal of Geophysical Research: Solid Earth, 105, B11, 26003-26016.

Canil, D., and Fedortchouk, Y. (2001) Olivine-liquid partitioning of vanadium and other trace elements, with applications to modern and ancient picrites. The Canadian Mineralogist, 39, 319-330.

Cherniak, D.J., and Watson, E.B. (2019) Al and Si diffusion in rutile. American Mineralogist, in press.

Cooper, L.B., Ruscitto, D.M., Plank, T., Wallace, P.J., Syracuse, E.M., and Manning, C.E. (2012) Global variations in H2O/Ce: I. Slab surface temperatures beneath volcanic arcs. Geochemistry Geophysics Geosystems, 13, 1-27.

Cottrell, E., and Kelley, K.A. (2011) The oxidation state of Fe in MORB glasses and the oxygen fugacity of the upper mantle. Earth and Planetary Science Letters, 305, 270-282.

Dasgupta, R., Jackson, M.G., and Lee, C.T.A. (2010) Major element chemistry of ocean island basalts—conditions of mantle melting and heterogeneity of mantle source. Earth and Planetary Science Letters, 289, 377-392.

Dickenson, M.P., and Hess, P.C. (1986) The structural role and homogeneous redox equilibria of iron in peraluminous, metaluminous and peralkaline silicate melts. Contributions to Mineralogy and Petrology, 92, 207-217.

Dingwell, D.B. (1992) Density of some titanium-bearing silicate liquids and the compositional dependence of the partial molar volume of TiO2. Geochimica et Cosmochimica Acta, 56, 3403-3407.

Dohmen, R., Marschall, H.R., Ludwig, T., and Polednia, J. (2018) Diffusion of Zr, Hf, Nb and Ta in rutile: effects of temperature, oxygen fugacity, and doping level, and relation to rutile point defect chemistry. Physics and Chemistry of Minerals, 1-22.

Donaldson, C.H. (1979) Composition changes in a basalt melt contained in a wire loop of Pt80Rh20: effects of temperature, time and oxygen fugacity. Mineralogical Magazine 43, 115-119.

Downs, R.T. (2006) The RRUFF Project: an integrated study of the chemistry, crystallography, Raman and infrared spectroscopy of minerals. Program and Abstracts of the 19th General Meeting of the International Mineralogical Association; Kobe, Japan.

Ducea, M.N., Saleeby, J.B., and Bergantz, G. (2015) The architecture, chemistry and evolution of continental magmatic arcs. Annual Review of Earth and Planetary Sciences, 43, 299-331.

Dygert, N., Liang, Y., and Hess, P. (2013) The importance of melt TiO_2 in affecting major and trace element partitioning between Fe-Ti oxides and lunar picritic glass melts. Geochimica et Cosmochimica Acta, 106, 134-151.

Elliott, T. (2003) Tracers of the slab. AGU Geophysical Monograph 138, 23-45.

Farges, F., Brown, G.E., and Rehr, J.J. (1996) Coordination chemistry of Ti (IV) in silicate glasses and melts: I. XAFS study of titanium coordination in oxide model compounds. Geochimica et Cosmochimica Acta, 60, 3023-3038.

Farges, F., and Brown, G.E. (1997) Coordination chemistry of titanium (IV) in silicate glasses and melts: IV. XANES studies of synthetic and natural volcanic glasses and tektites at ambient temperature and pressure. Geochimica et Cosmochimica Acta, 61, 1863-1870.

Frost, D.J., and McCammon, C.A. (2008) The redox state of the Earth's mantle. Annual Reviews in Earth and Planetary Science, 36, 389-420.

Foley, S.F., Barth, M.G., and Jenner, G.A. (2000) Rutile/melt partition coefficients for trace elements and an assessment of the influence of rutile on the trace element characteristics of subduction zone magmas. Geochimica et Cosmochimica Acta, 64, 933-938.

Gaetani, G.A., Asimow, P.D., and Stolper, E.M. (2008) A model for rutile saturation in silicate melts with applications to eclogite partial melting in subduction zones and mantle plumes. Earth and Planetary Science Letters, 272, 720-729.

Gale, A., Dalton, C.A., Langmuir, C.H., Su, Y., and Schilling, J. (2013) The mean composition of ocean ridge basalts. Geochemistry, Geophysics, Geosystems, 14, 489-518.

Gill, J. B. (1981) Orogenic Andesites and Plate Tectonics. Springer-Verlag, Berlin.

Greegor, R.B., Lytle, W.B., Sandstrom, D.R., Wong, J., and Schultz, P. (1983) Investigation of TiO_2-SiO_2 glasses by X-ray absorption spectroscopy. Journal of Non-Crystalline Solids, 55, 27-43.

Green, T.H. (2000) New partition coefficient determinations pertinent to hydrous melting processes in subduction zones. In State of the Arc 2000: Processes and Timescales (eds. J.P. Davidson, J.A. Davidson and R.C. Price). Carolyn Bain Publishing House, Wellington, pp.92-95.

Green, T.H., and Pearson, N.J. (1986) Ti-rich accessory phase saturation in hydrous mafic-felsic compositions at high P, T. Chemical Geology, 54, 185-201.

Green, T.H., and Pearson, N.J. (1987) An experimental study of Nb and Ta partitioning between Ti-rich minerals and silicate liquids at high temperature and pressure. Geochimica et Cosmochimica Acta, 51, 55-62.

Grove, T.L. (1982) Use of FePt alloys to eliminate the iron loss problem in 1 atmosphere gas mixing experiments: Theoretical and practical considerations. Contributions to Mineralogy and Petrology, 78, 298-304.

Guignard, M., Cormier, L., Montouillout, V., Menguy, N., and Massiot, D. (2010) Structural fluctuations and role of Ti as nucleating agent in an aluminosilicate glass. Journal of Non-Crystalline Solids, 356, 1368-1373.

Guo, S., Tang, P., Su, B., Chen, B., Ye, K., Zhang, L., Gao, Y., Liu, J., and Yang, Y. (2017) Unusual replacement of Fe-Ti oxides by rutile during retrogression in amphibolite-hosted veins (Dabie UHP terrane): A mineralogical record of fluid-induced oxidation processes in exhumed UHP slabs. American Mineralogist, 102, 2268-2283.

Hermann, J. (2002) Allanite: thorium and light rare earth element carrier in subducted crust. Chemical Geology, 192, 289-306.

Hermann, J., and Rubatto, D. (2009) Accessory phase control on the trace element signature of sediment melts in subduction zones. Chemical Geology, 265, 512-526.

Hills, D.V., and Haggerty, S.E. (1989) Petrochemistry of eclogites from the Koidu kimberlite complex, Sierra Leone. Contributions to Mineralogy and Petrology, 1989, 397-422.

Hoff, C.M. (2019) Defect thermometry using rutile and feldspar. Ph.D. thesis, Rensselaer Polytechnic Institute.

Holycross, M.E., and Watson, E.B. (2016) Diffusive fractionation of trace elements in basaltic melts. Contributions to Mineralogy and Petrology, 171, 80-95.

Holycross, M.E., and Watson, E.B. (2018) Trace element diffusion and kinetic fractionation in wet rhyolitic melt. Geochimica et Cosmochimica Acta, 232, 14-29.

Horng, W.S., and Hess, P.C. (2000) Partition coefficients of Nb and Ta between rutile and anhydrous haplogranite melts. Contributions to Mineralogy and Petrology, 138, 176-185.

Jenner, G.A., Foley, S.F., Jackson, S.E., Green, T.H., Fryer, B.J., and Longerich, H.P. (1993) Determination of partition coefficients for trace elements in high pressure-temperature experimental run products by laser ablation microprobe-inductively coupled plasma-mass spectrometry (LAM-ICP-MS). Geochimica et Cosmochimica Acta, 58, 5099-5103.

John, T., Klemd, R., Klemme, S., Pfander, J.A., Hoffmann, J.E., and Gao, J. (2011) Nb-Ta fractionation by partial melting at the titanite-rutile transition. Contributions to Mineralogy and Petrology, 161, 35-45.

Kelemen, P.B., Hanghoj, K., and Greene, A.R. (2003) One view of the geochemistry of subduction-related magmatic arcs, with an emphasis on primitive andesite and lower crust. Treatise on Geochemistry, 3, 659.

Klemme, S., Blundy, J.D., and Wood, B.J. (2002) Experimental constraints on major and trace element partitioning during partial melting of eclogite. Geochimica et Cosmochimica Acta, 66, 3109-3123.

Klemme, S., Prowatke, S., Hametner, K., and Günther, D. (2005) Partitioning of trace elements between rutile and silicate melts: implications for subduction zones. Geochimica et Cosmochimia Acta, 69, 2361-2371.

Kofstad, P. (1972) Nonstoichiometry, diffusion and electrical conductivity in binary metal oxides. Wiley, New York.

Kylander-Clark, A.R.C., Hacker, B.R., and Mattinson, J.M. (2008) Slow exhumation of UHP terranes: titanite and rutile ages of the Western Gneiss Region, Norway. Earth and Planetary Science Letters, 272, 531-540.

Laubier, M., Grove, T.L., and Langmuir C.H. (2014) Trace element mineral/melt partitioning for basaltic and basaltic andesitic melts: An experimental and laser ICP-MS study with application to the oxidation state of mantle source regions. Earth and Planetary Science Letters, 392, 265-278.

Lanzirotti, A., Dyar, M.D., Sutton, S., Newville, M., Head, E., Carey, C.J., McCanta, M., Lee, L. King, P.L., and Jones, J. (2018) Accurate predictions of microscale oxygen barometry in basaltic glasses using V K-edge X-ray absorption spectroscopy: A multivariate approach. American Mineralogist, 103, 1282-1297

Lee, C.T.A., Leeman, W.P., Canil, D., and Li, Z.X.A. (2005) Similar V/Sc systematics in MORB and arc basalts: implications for the oxygen fugacities of their mantle source regions. Journal of Petrology, 46, 2313-2336.

Lee, C.T., Cheng, X., and Horodyskyj, U. (2006) The development and refinement of continental arcs by primary basaltic magmatism, garnet pyroxenite accumulation, basaltic recharge and delamination: insights from the Sierra Nevada, California. Contributions to Mineralogy and Petrology, 151, 222-242.

Leitzke, F.P., Fonesca, R.O.C., Michely, L.T., Sprung, P., Munker, C., Heuser, A., and Blanchard, H. (2016) The effect of titanium on the partitioning behavior of high-field strength elements between silicates, oxides and lunar basaltic melts with applications to the origin of mare basalts. Chemical Geology, 440, 219-238.

Lietzke, F.P., Fonesca, R.O.C., Göttlicher, J., Steininger, R., Jahn, S., Prescher, C., and Lagos, M. (2018) Ti K-edge XANES study on the coordination number and oxidation state of titanium in pyroxene, olivine, armacolite, ilmenite and silicate glass during mare basalt petrogenesis. Contributions to Mineralogy and Petrology, 173, 103.

Liou, J.G., Zhang, R., Ersnt, W.G., Liu, J., and McLimans, R. (1998) Mineral paragenesis in the Pianpalaudo eclogitic body, Gruppo di Voltri, western Ligurian Alps. Schweizerische Mineralogische und Petrographische Mitteilungen, 78, 317-335.

Liu, L., Xiao, Y., Aulbach, S., Li, D., and Hou, Z. (2014) Vanadium and niobium behavior in rutile as a function of oxygen fugacity: evidence from natural samples. Contributions to Mineralogy and Petrology, 167, 1026.

Luvizotto, G.L., Zack, T., Meyer, H.P., Ludwig, T., Treibold, S., Kronz, A., Munker, C., Stockli, D.F., Prowatke, S., Klemme, S., Jacob, D.E., and von Eynatten, H. (2009) Rutile crystals as potential trace element and isotope mineral standard for microanalysis. Chemical Geology, 261, 346-369.

Mallmann, G., and O'Neill, H.S.C. (2007) The effect of oxygen fugacity on the partitioning of Re between crystals and silicate melt during mantle melting. Geochimica et Cosmochimica Acta, 71, 2837-2857.

Mallmann, G., and O'Neill, H.S.C. (2009) The crystal/melt partitioning of V during mantle melting as a function of oxygen fugacity compared with some other elements (Al, P, Ca, Sc, Ti, Cr, Fe, Ga, Y, Zr and Nb). Journal of Petrology, 50, 1765-1794.

Mallmann, G., Fonesca, R.O.C., and Silva, A.B. (2014) An experimental study of the partitioning of rutile and silicate melt as a function of oxygen fugacity. Anais da Academia Brasileira de Ciências, 86, 1609-1629.

Marschall, H.R., Dohmen, R., and Ludwig, T. (2013) Diffusion-induced fractionation of niobium from tantalum during continental crust formation. Earth and Planetary Science Letters, 375, 361-371.

McCallum, I.S., and Charette, M.P (1978) Zr and Nb partition coefficients: implications for the genesis of mare basalts, KREEP and sea floor basalts. Geochimica et Cosmochimica Acta 42, 859-869.

Meinhold, G. (2010) Rutile and its applications in earth sciences. Earth-Science Reviews, 102, 1-28.

Mysen, B.O. (1983) The structure of silicate melts. Annual Review of Earth and Planetary Sciences, 11, 7597.

Nowotny, M.K., Sheppard, L.R., Bak, T., and Nowotny, J. (2008) Defect chemistry of titanium dioxide. Application of defect engineering in processing TiO2-based photocatalysts. Journal of Physical Chemistry C, 112, 5275-5300.

O'Neill, H.S.C. (1987) Quartz-fayalite-iron and quartz-fayalite-magnetite equilibria and the free energy of formation of fayalite (Fe2SiO4) and magnetite (Fe3O4). American Mineralogist 72, 67-75

O'Neill, H.S.C., Berry, A.J., and Mallmann, G. (2018) The oxidation state of iron in Mid-Ocean Ridge Basaltic (MORB) glasses: implications for their petrogenesis and oxygen fugacities. Earth and Planetary Science Letters, 504, 152-162.

Papike, J.J., Simon, S.B., Burger, P.V., Bell, A.S., Shearer, C.K., and Karner, J.M. (2016) Chromium, vanadium, and titanium valence systematics in Solar System pyroxene as a recorder of oxygen fugacity, planetary provenance, and processes. American Mineralogist, 101, 907-918.

Paton, C., Hellstrom, J., Paul, B., Woodhead, J., and Hergt, J. (2011) Iolite: Freeware for the visualization and processing of mass spectrometric data. Journal of Analytical Atomic Spectrometry, 26, 2508-2518.

Pearce, N.J., Perkins, W.T., Westgate, J.A., Gorton, M.P., Jackson, S.E., Neal, C.R., and Chenery, S.P. (1997) A compilation of new and major published major and trace element trace element data for NIST SRM 610 and NIST SRM 612 glass reference materials. Geostandards Newsletter, 21, 115-144.

Plank, T., Cooper, L.B., and Manning, C.E. (2009) Emerging geothermometers for estimating slab surface temperatures. Nature Geoscience, 2, 611-615.

Rapp, R.P. and Watson, E. B. (1995) Dehydration melting of metabasalt at 8-32 kbar: implications for continental growth and crust-mantle recycling. Journal of Petrology 36, 891-931.

Righter, K., Sutton, S., Danielson, L., Pando, K., Schmidt, G., Yang, H., Berthet, S., Newville, M., Choi, Y., Downs, R.T., and Malavergne, V. (2011) The effect of fO2 on the partitioning and valence of V and Cr in garnet/melt pairs and the relation to terrestrial mantle V and Cr content. American Mineralogist, 96, 1278-1290.

Rodriguez-Vargas, A., Koester, E., Mallmann, G., Conceição, R.V., Kawashita, K., and Weber M.B.I. (2005) Mantle diversity beneath the Colombian Andes, Northern Volcanic Zone: Constraints from Sr and Nd isotopes. Lithos, 82, 471-484.

Romano, C., Paris, E., Poe, B.T., Giuli, G., Dingwell, D.B., and Mottana, A. (2000) Effect of aluminum of Ti-coordination in silicate glasses: A XANES study. American Mineralogist, 85, 108-117.

Rudnick, R.L., Barth, M., Horn, I., and McDonough, W.F. (2000) Rutile-bearing refractory eclogites: missing link between continents and the depleted mantle. Science, 287, 278-281.

Ryerson, P.J., and Hess, P.C. (1978) Implications of liquid-liquid distribution coefficients to mineral-liquid partitioning. Geochimica et Cosmochimica Acta, 42, 921-932.

Ryerson, F.J., and Watson, E.B. (1987) Rutile saturation in magmas: implications for Ti-Nb-Ta depletion in island-arc basalts. Earth and Planetary Science Letters, 86, 225-239.

Schmidt, M.W., Dardon, A., Chazot, G., and Vannucci, R. (2004) The dependence of Nb and Ta rutile-melt partitioning on melt composition and Nb/Ta fractionation during subduction processes. Earth and Planetary Science Letters, 226, 415-432.

Shannon, R.D. (1976) Revised effective ionic radii and systematic studies of interatomic distances in halides and chalcogenides. Acta Crystallography, 32, 751-766.

Shervais, J.W. (1982) Ti-V plots and the petrogenesis of modern and ophiolitic lavas. Earth and Planetary Science Letters, 59, 101-118.

Shishkina, T.A., Portnyagin, M.V., Botcharnikov, R.E., Almeev, R.R., Simonyan, A.V., Garbe-Shönberg, D., Schuth, S., Oeser, M. and Holtz, F. (2018) Experimenal calibration and implications of olivine-melt vanadium oxybarometry for hydrous basaltic arc magmas. American Mineralogist, 103, 369-383.

Sisson, T.W., and Kelemen, P.B. (2018) Near-solidus melts of MORB + 4 wt% H2O at 0.8-2.8 GPa applied to issues of subduction magmatism and continent formation. Contributions to Mineralogy and Petrology, 173, 70-93.

Snetsinger, K.G., Bunch, T.E. and Keil, K. (1968) Electron microprobe analysis of vanadium in the presence of titanium. American Mineralogist 53, 1770-1773.

Sossi, P.A., and O'Neill, H.S.C. (2016) Liquidus temperatures of komatiites and the effect of cooling rate on element partitioning between olivine and komatiitic melt. Contributions to Mineralogy and Petrology, 171, 49-74.

Sossi, P.A., Prytulak, J., and O'Neill, H.S.C. Experimental calibration of vanadium partitioning and stable isotope fractionation between hydrous granitic melt and magnetite at 800 C and 0.5 GPa. Contributions to Mineralogy and Petrology, 173, 27-45.

Stolper, D.A., and Bucholz, C.E. (2019) Neoproterozoic to early Phanerozoic rise in island arc redox state due to deep ocean oxygenation and increased marine sulfate levels. Proceedings of the National Academy of Sciences, 116, 8746-8755.

Sutton, S.R., Karner, J., Papike, J., Delaney, J.S., Shearer, C., Newville, M., Eng, P., Rivers, M., and Dyar, M.D. (2005) Vanadium K edge XANES of synthetic and natural basaltic glasses and application to microscale oxygen barometry. Geochimica et Cosmochimica Acta 69, 2333-2348.

Syracuse, E.M., van Keken, P.E. and Abers, G.A. (2010) The global range of subduction zone thermal models. Physics of the Earth and Planetary Interiors, 183, 73-90.

Tang, M., Lee, C.T.A., Chen, K., Erdman, M., Costin, G., and Jiang, H. (2019) Nb/Ta systematics in arc magma differentiation and the role of arclogites in continent formation. Nature Communications, 10, 235.

Toplis, M.J. and Corgne, A. (2002) An experimental study of element partitioning between magnetite, clinopyroxene and iron-bearing silicate liquids with a particular emphasis on vanadium. Contributions to Mineralogy and Petrology, 144, 22-37.

Trail, D., Tailby, N., Wang, Y., Harrison, T.M., and Boehnke, P. (2017) Aluminum in zircon as evidence for peraluminous and metaluminous melts from the Hadean to present. Geochmistry, Geophysics, Geosystems, 18, 1580-1593.

Turner, S.J., and Langmuir, C.H. (2015) What processes control the chemical compositions of arc front stratovolcanoes? Geochemistry, Geophysics, Geosystems, 16, 1865-1893.

van Keken, P.E., Kiefer, P.B., and Peacock, S.M. (2002) High-resolution models of subduction zones: implications for mineral dehydration reactions and transport of water into the deep mantle. Geochemistry Geophysics Geosystems, 3, 1056.

Walker, D., Juerwicz, S., and Watson, E.B. (1988) Adcumulus dunite growth in a laboratory thermal-gradient. Contributions to Mineralogy and Petrology, 99, 306-319.

Wang, J., Xiong, X., Takahashi, E., Zhang, L., Li, L., and Liu, X. (2019) Oxidation state of the arc mantle revealed by partitioning of V, Sc, and Ti between mantle minerals and basaltic minerals. Journal of Geophysical Research, in press.

Watson, E.B. (1976) Two-liquid partition coefficients: experimental data and geochemical implications. Contributions to Mineralogy and Petrology, 56, 119-134.

Watson, E.B., and Müller, T. (2009) Non-equilibrium isotopic and elemental fractionation during diffusion-controlled crystal growth under static and dynamic conditions. Chemical Geology, 267, 111-124.

Wendlandt, R.F. (1990) Partitioning of niobium and tantalum between rutile and silicate melt. EOS AGU Fall Meeting 71, 1658.

Wood, B.J., and Blundy, J.D. (2002) The effect of H2O on crystal-melt partitioning of trace elements. Geochimica et Cosmochimica Acta,66, 3647-3656.

Xiao, Y., Sun, W., Hoefs, J., Simon, K., Zhang, Z., Li, S., and Hofmann, A.W. (2006) Making continental crust through slab melting: constraints from niobium-tantalum fractionation in UHP metamorphic rutile. Geochimica et Cosmochimica Acta, 70, 4770-4782.

Xiong, X.L., Adam, J., and Green, T.H. (2005) Rutile stability and rutile/melt HFSE partitioning during partial melting of hydrous basalt: implications for TTG genesis. Chemical Geology, 218, 339-359.

Xiong, X., Keppler, H., Audetat, A., Gudfinnsson, G., Sun, W., Song, M., Xiao, W., and Yuan, L. (2009) Experimental constraints on rutile saturation during partial melting of metabasalt at the amphibolite to eclogite transition, with application to TTG genesis. American Mineralogist, 94, 1175-1186.

Xiong, X., Keppler, H., Audetat, A., Ni, H., Sun, W., and Li, W. (2011) Partitioning of Nb and Ta between rutile and felsic melt and the fractionation of Nb/Ta during partial melting of hydrous metabasalt. Geochimica et Cosmochimica Acta, 75, 1673-1692.

Zack, T., Kronz, A., Foley, S.F. and Rivers, T. (2002) Trace element abundances in rutiles from eclogites and associated garnet mica schists. Chemical Geology, 184, 97-122.

Zack, T., and Kooijman, E. (2017) Petrology and geochronology of rutile. Reviews in Mineralogy and Geochemistry, 83, 443-467.

Zhang, H.L., Cottrell, E., Solheid, P.A., Kelley, K.A., and Hirschmann, M.M. (2018) Determination of $Fe^{3+}/\Sigma Fe$ of XANES basaltic glass standards by Mössbauer spectroscopy and its application to the oxidation state of iron in MORB. Chemical Geology, 479, 166-175.

Xirouchakis, D., Hirschmann, M.M., and Simpson, J.A. (2001) The effect of titanium on the silica content and on mineral-liquid partitioning of mantle-equilibrated melts. Geochimica et Cosmochimica Acta, 65, 2201-2217.

This is a preprint, the final version is subject to change, of the American Mineralogist (MSA)
Cite as Authors (Year) Title. American Mineralogist, in press.
DOI: https://doi.org/10.2138/am-2020-7013

Figure Captions

Figure 1 Average vanadium valence as a function of oxygen fugacity in silicate glass standards measured via X-ray absorption near edge structure (XANES) spectroscopy. Vanadium data is temperature corrected as measured by Sutton et al. (2005). Transition from V^{4+} to higher oxidation states occurs at ~QFM-2. The position of "air" is calculated at 1300 ºC.

Figure 2 Optical microscope view of rutile grains and glass in thin sections made from experiments at fO_2=QFM and 1300 °C. a) MORBTi composition b) DacTi composition and c) LCOTi composition. Grains become more acicular as melt polymerization increases.

Figure 3 Rutile saturation in silicate melts at 1 atm pressure is strongly correlated with melt polymerization and temperature. The studies of Mallmann et al. (2014) and Klemme et al. (2005) were conducted at temperatures comparable to this study (T=1250-1300 °C). The rutile saturation experiments of Gaetani et al. 2008 (dark gray squares) extended to 1450 °C. We parameterized the relationship between rutile solubility and melt composition to minimize the amount of TiO_2 in our melts at rutile saturation.

Figure 4 Rutile/melt partitioning of V at 1300 °C and one atm as a function of oxygen fugacity. Values of $D_V^{rt/melt}$ change with melt polymerization, parameterized as NBO/T (Mysen 1983). Unseen error bars are smaller than the size of data points. Curves are fit to the data using equation 5.

Figure 5 Comparison of this study to literature data examining rutile/melt partitioning of V at one atm pressure and T=1250-1300 °C. In contrast to Mallmann et al. (2014) and Klemme et al. (2005), we do not find any conditions where V becomes incompatible in rutile. Error bars smaller than the size of data points when unseen. Curves are fit to the data using equation 5.

Figure 6 Partitioning of V between rutile and melt at constant fO_2 is dependent on melt composition. The relationship between $D_V^{rt/melt}$ and composition may be expressed as a function of (a) melt polymerization or (b) melt TiO_2 content. Curves define an exponential relationship. See discussion in text for more detail.

Figure 7 Spider diagram showing trace element partitioning between rutile and melt for three experiments (DacTi and MORBTi at QFM-1 and MORBTi at QFM-2). Elements are arranged in order of compatibility (Hofmann 1988). Increasing melt polymerization increases $D^{rt/melt}$ for all cations investigated here—note that decreasing fO_2 increases melt polymerization slightly in the MORBTi experiments due to increased volatilization of Na (e.g., Donaldson 1979). Experiments conducted at higher oxygen fugacities grew rutile that were insufficient in size for LA-ICP-MS. Error bars smaller than data points where unseen.

Figure 8 The addition of rutile to refractory eclogite residues reduces the amount of Ti and V transferred from the slab to the overlying arc in subduction zones. **a)** Vanadium content of slab melts at F=5% (i.e., 5% partial melting) as a function of mineral assemblage and fO_2. Melts from eclogites containing only garnet and clinopyroxene will contain more V than melts from rutile-bearing residues. The retention of V in the mineral residue is greatest at the fO_2s (<QFM) where

This is a preprint, the final version is subject to change, of the American Mineralogist (MSA)
Cite as Authors (Year) Title. American Mineralogist, in press.
DOI: https://doi.org/10.2138/am-2020-7013

V is the most compatible in rutile. **b)** The Ti/V ratios of eclogite slab melts change as a function of oxygen fugacity and mineral assemblage. Ti partitioning is constant over the modeled fO_2 range. Slab melting will not contribute a Ti/V component to the overlying arc that is less than the Ti/V of MORB unless the refractory slab assemblage contains >1 wt% rutile and slab melting occurs at *f*O2s≥QFM. See text for more detail.

This is a preprint, the final version is subject to change, of the American Mineralogist (MSA)
Cite as Authors (Year) Title. American Mineralogist, in press.
DOI: https://doi.org/10.2138/am-2020-7013

Table 1 Compositions of experimental starting materials

oxide (wt%)	MORBTi	DacTi	LCOTi
SiO_2	36.27	55.52	68.82
TiO_2	31.24	16.59	10.72
Al_2O_3	8.99	12.62	11.25
FeO	6.45	3.38	0.67
MgO	6.18	1.68	0.06
CaO	7.86	4.21	0.43
Na_2O	2.14	3.36	3.63
K_2O	0.15	2.10	3.94
V_2O_3	0.40	0.38	0.36
TE (all)	0.12	0.16	0.13
NBO/T	0.71	0.21	0.03

Table 2 Experiment conditions and measured rutile/melt partition coefficients for vanadium. All experiments were conducted at 1300 ºC and 1 atm pressure.

composition	fO_2 (ΔQFM)	time (hr)	run products	NBO/T melt	TiO_2 melt	$D_V^{rt/melt}$	σ
MORBTi	-2	136.5	rutile, melt	0.66	16.56	3.87	0.05
MORBTi	-1	126.0	rutile, melt	0.64	16.06	3.50	0.04
MORBTi	0	111.3	rutile, melt	0.70	18.16	2.65	0.03
MORBTi	2	42.9	rutile, melt	0.74	19.36	1.81	0.03
MORBTi	6.54 (air)	67.3	rutile, armacolite, melt	0.47	14.51	1.11	0.04
DacTi	-2	72.4	rutile, melt	0.12	7.22	14.02	0.02
DacTi	-1	116.3	rutile, melt	0.14	7.15	10.25	0.05
DacTi	0	101.5	rutile, melt	0.13	7.37	7.08	0.02
DacTi	1	40.0	rutile, melt	0.14	7.51	5.01	0.03
DacTi	1	231.7	rutile, melt	0.13	7.84	5.05	0.03
DacTi	2	66.9	rutile, melt	0.17	8.14	3.87	0.02
DacTi	6.54 (air)	50.3	rutile, melt	0.19	8.71	1.50	0.03
LCOTi	-1	126.0	rutile, melt	0.00	5.30	21.79	0.05
LCOTi	0	88.7	rutile, melt	0.00	5.38	17.27	0.06
LCOTi	1	237.1	rutile, melt	0.00	8.74	9.12	0.08
LCOTi	6.54 (air)	67.3	rutile, melt	0.00	7.40	1.68	0.06

This is a preprint, the final version is subject to change, of the American Mineralogist (MSA)
Cite as Authors (Year) Title. American Mineralogist, in press.
DOI: https://doi.org/10.2138/am-2020-7013

Table 3 Rutile/melt trace element partition coefficients at 1300 °C and 1 atm.

composition	MORBTi		MORBTi		DacTi	
fO_2 **(ΔQFM)**	-2		-1		-2	
element	$D^{rt/melt}$	**σ**	$D^{rt/melt}$	**σ**	$D^{rt/melt}$	**σ**
Sc	0.31	0.03	0.30	0.01	1.30	0.13
Cr	14.81	2.16	17.19	1.54	44.96	3.03
Mn	0.00	0.00	0.01	0.00	0.10	0.06
Fe	0.01	0.01	0.06	0.00	0.10	0.05
Ni	--	--	0.15	0.02	--	--
Y	1.48E-02	1.99E-03	1.43E-02	2.00E-03	0.11	0.09
Zr	3.90	0.26	3.63	0.12	10.53	0.41
Nb	45.34	3.44	39.29	2.19	120.04	8.14
La	--	--	2.02E-03	2.45E-03	0.13	0.06
Ce	9.96E-04	2.01E-05	3.42E-03	2.78E-03	0.12	0.05
Pr	3.64E-04	9.92E-06	2.58E-03	1.87E-03	0.13	0.07
Nd	4.82E-03	2.31E-03	4.80E-03	1.52E-03	0.13	0.06
Sm	6.51E-03	1.43E-04	4.03E-03	3.13E-03	0.09	0.08
Eu	1.36E-03	3.43E-05	3.26E-03	2.32E-03	0.14	0.05
Gd	3.37E-03	1.62E-04	6.65E-03	4.18E-03	0.15	0.08
Dy	2.24E-03	8.91E-04	3.26E-03	2.15E-03	0.15	0.06
Ho	2.08E-03	5.19E-04	2.91E-03	2.02E-03	0.11	0.09
Er	5.07E-03	1.96E-03	4.70E-03	1.38E-03	0.11	0.09
Yb	6.13E-03	1.74E-04	7.29E-03	2.37E-03	0.14	0.10
Lu	9.20E-03	1.06E-03	8.82E-03	2.38E-03	0.15	0.11
Hf	5.96	0.31	5.62	0.28	14.69	1.34
Ta	115.05	14.11	55.83	11.21	218.36	39.79

This is a preprint, the final version is subject to change, of the American Mineralogist (MSA)
Cite as Authors (Year) Title. American Mineralogist, in press.
DOI: https://doi.org/10.2138/am-2020-7013

Figure 1

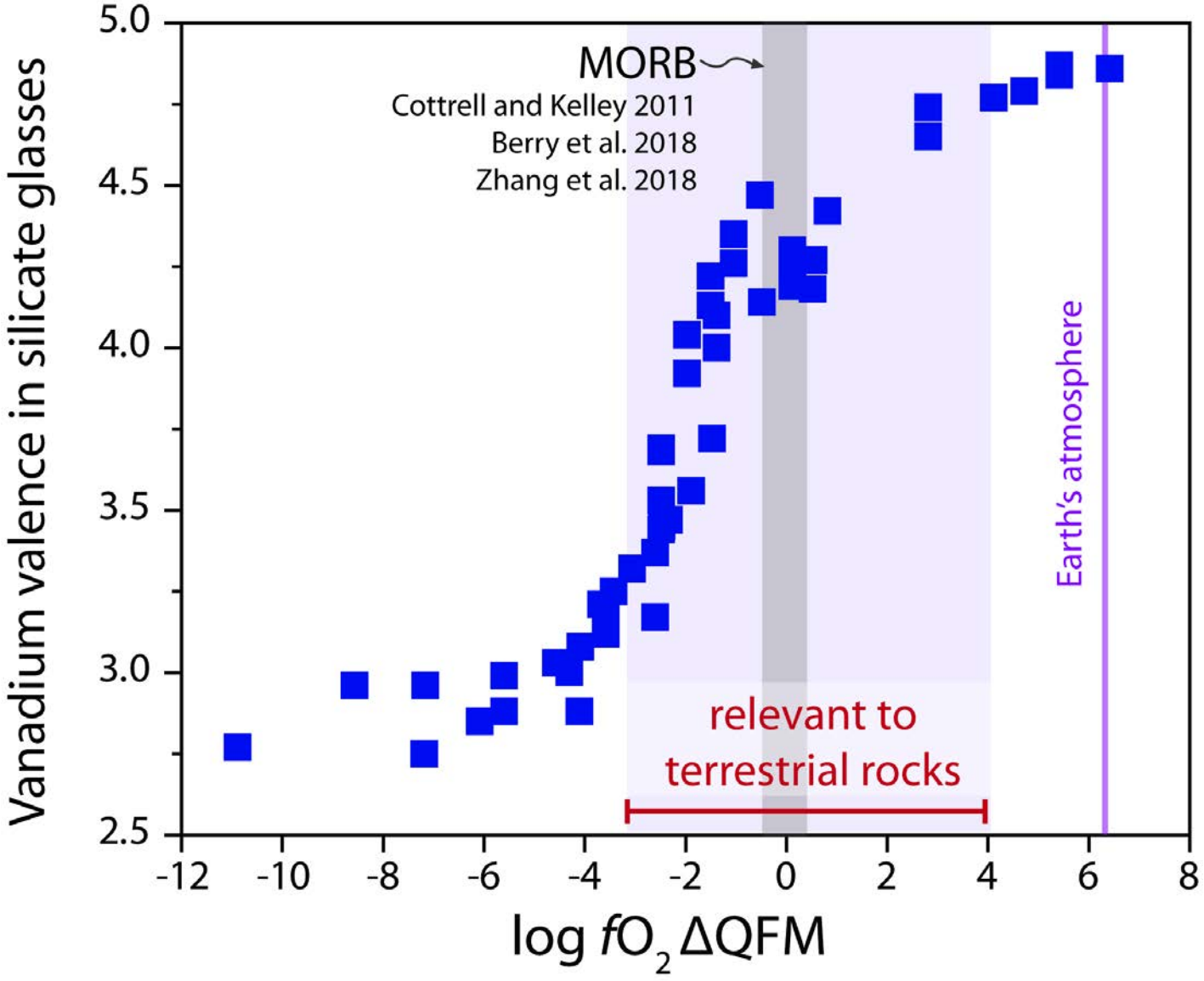

This is a preprint, the final version is subject to change, of the American Mineralogist (MSA)
Cite as Authors (Year) Title. American Mineralogist, in press.
DOI: https://doi.org/10.2138/am-2020-7013

Figure 2

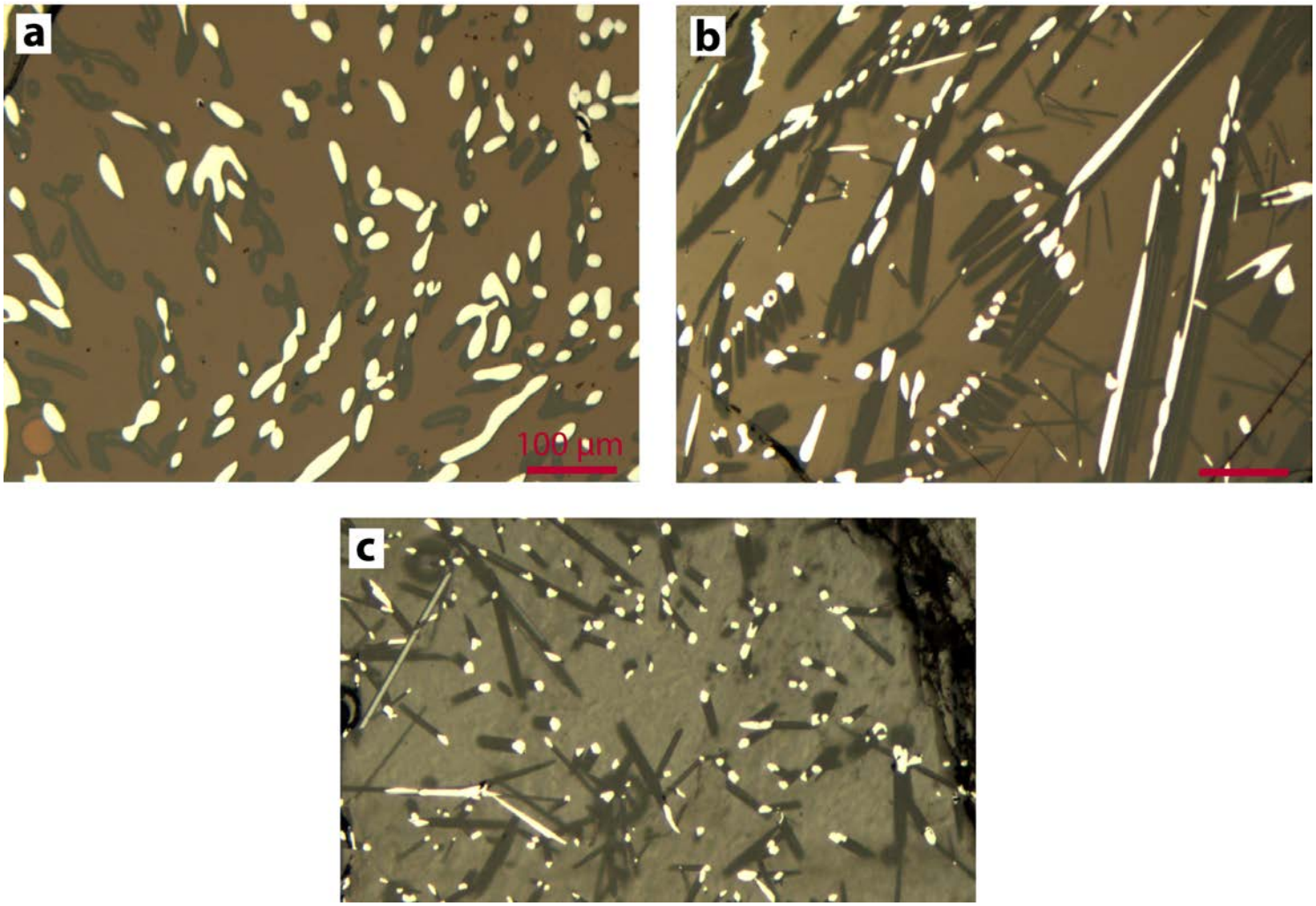

This is a preprint, the final version is subject to change, of the American Mineralogist (MSA)
Cite as Authors (Year) Title. American Mineralogist, in press.
DOI: https://doi.org/10.2138/am-2020-7013

Figure 3

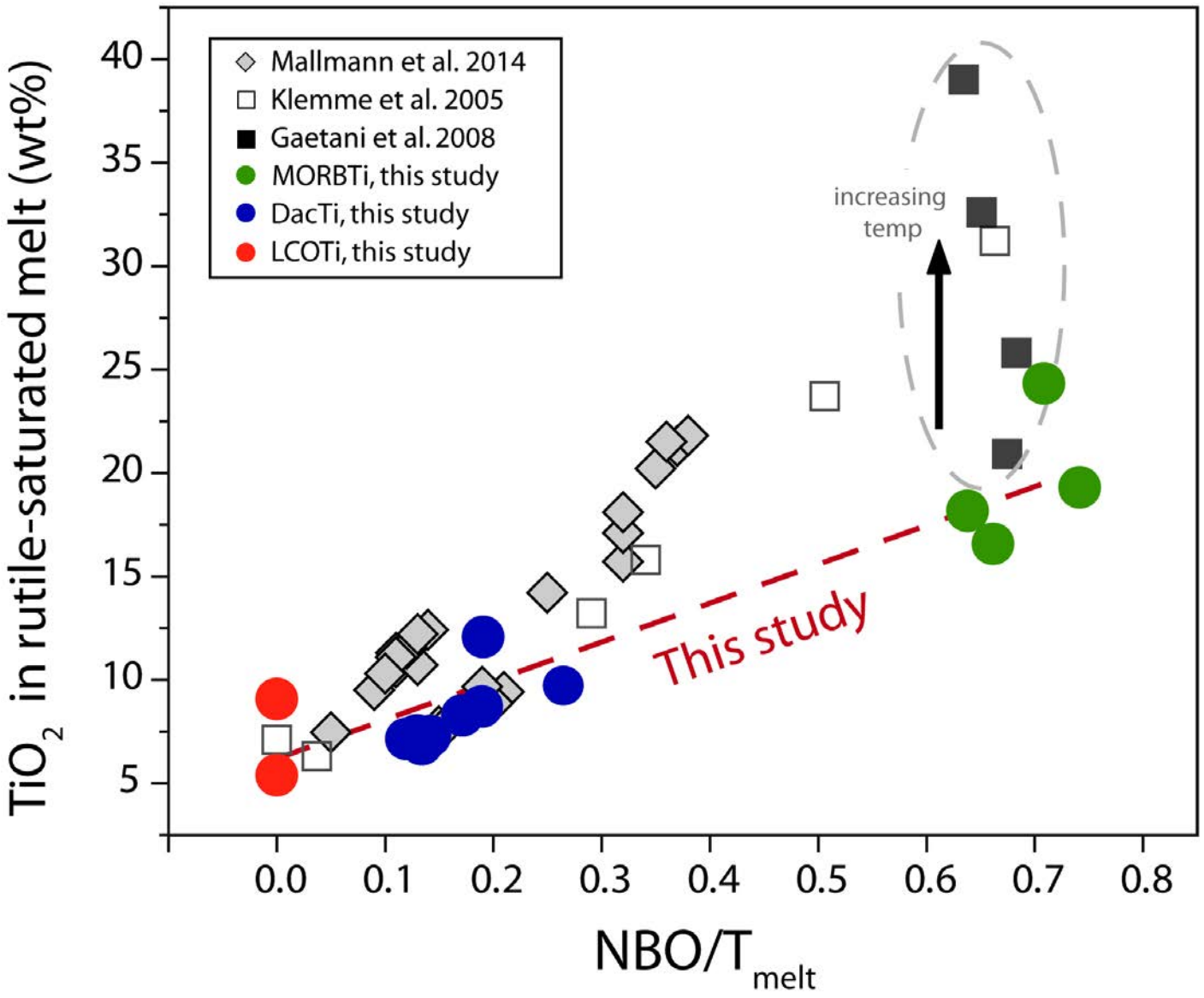

This is a preprint, the final version is subject to change, of the American Mineralogist (MSA)
Cite as Authors (Year) Title. American Mineralogist, in press.
DOI: https://doi.org/10.2138/am-2020-7013

Figure 4

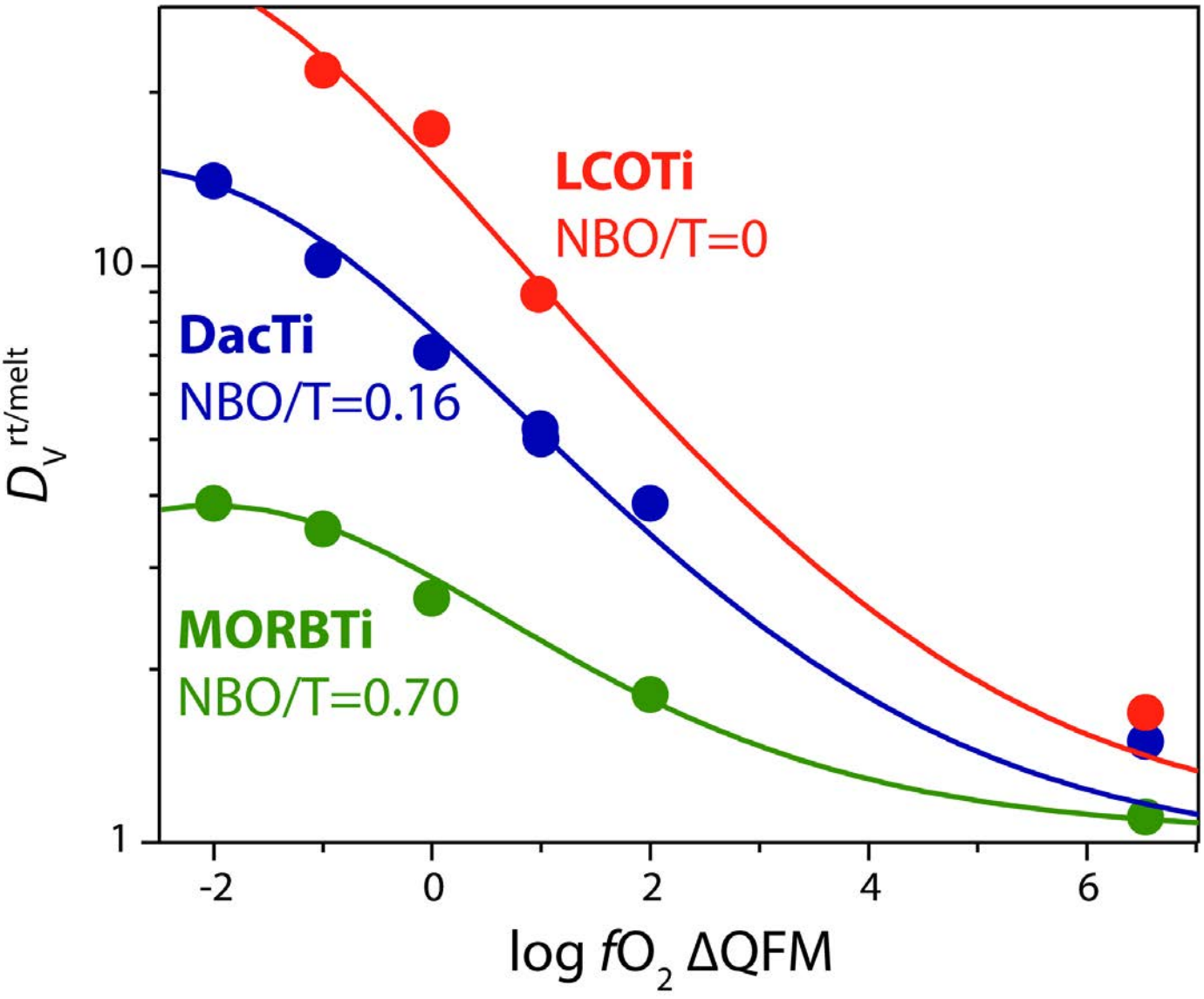

This is a preprint, the final version is subject to change, of the American Mineralogist (MSA)
Cite as Authors (Year) Title. American Mineralogist, in press.
DOI: https://doi.org/10.2138/am-2020-7013

Figure 5

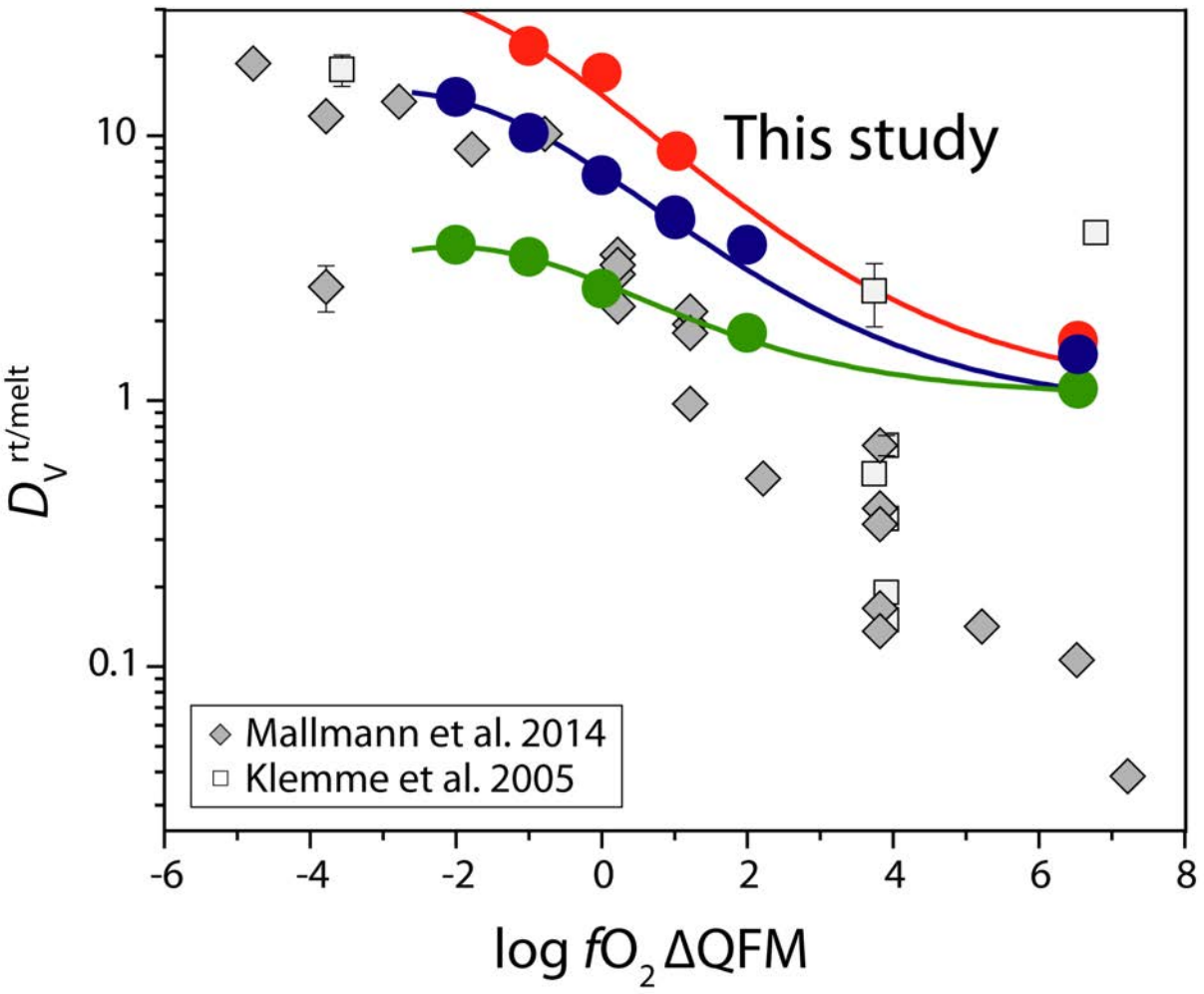

This is a preprint, the final version is subject to change, of the American Mineralogist (MSA)
Cite as Authors (Year) Title. American Mineralogist, in press.
DOI: https://doi.org/10.2138/am-2020-7013

Figure 6

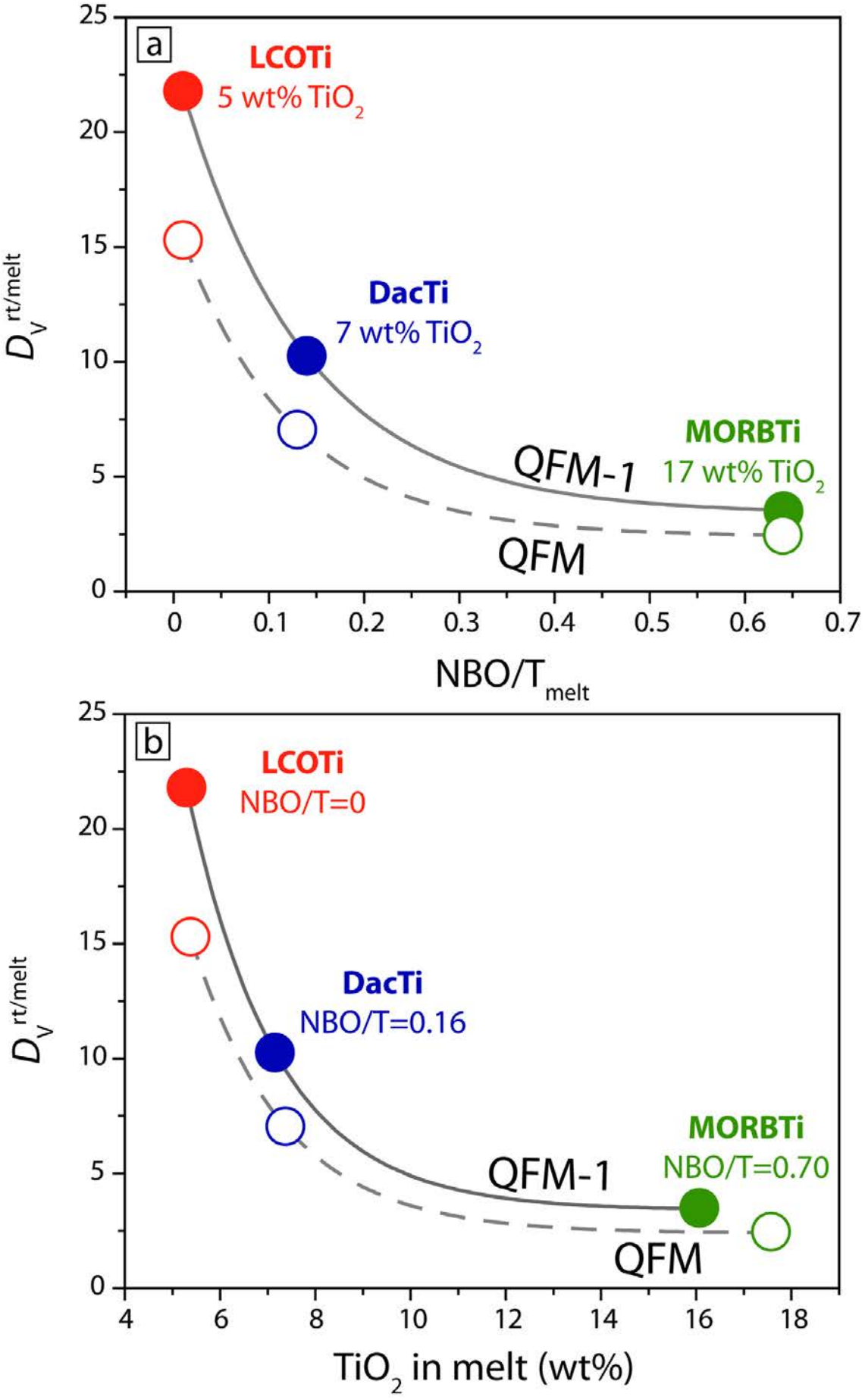

This is a preprint, the final version is subject to change, of the American Mineralogist (MSA)
Cite as Authors (Year) Title. American Mineralogist, in press.
DOI: https://doi.org/10.2138/am-2020-7013

Figure 7

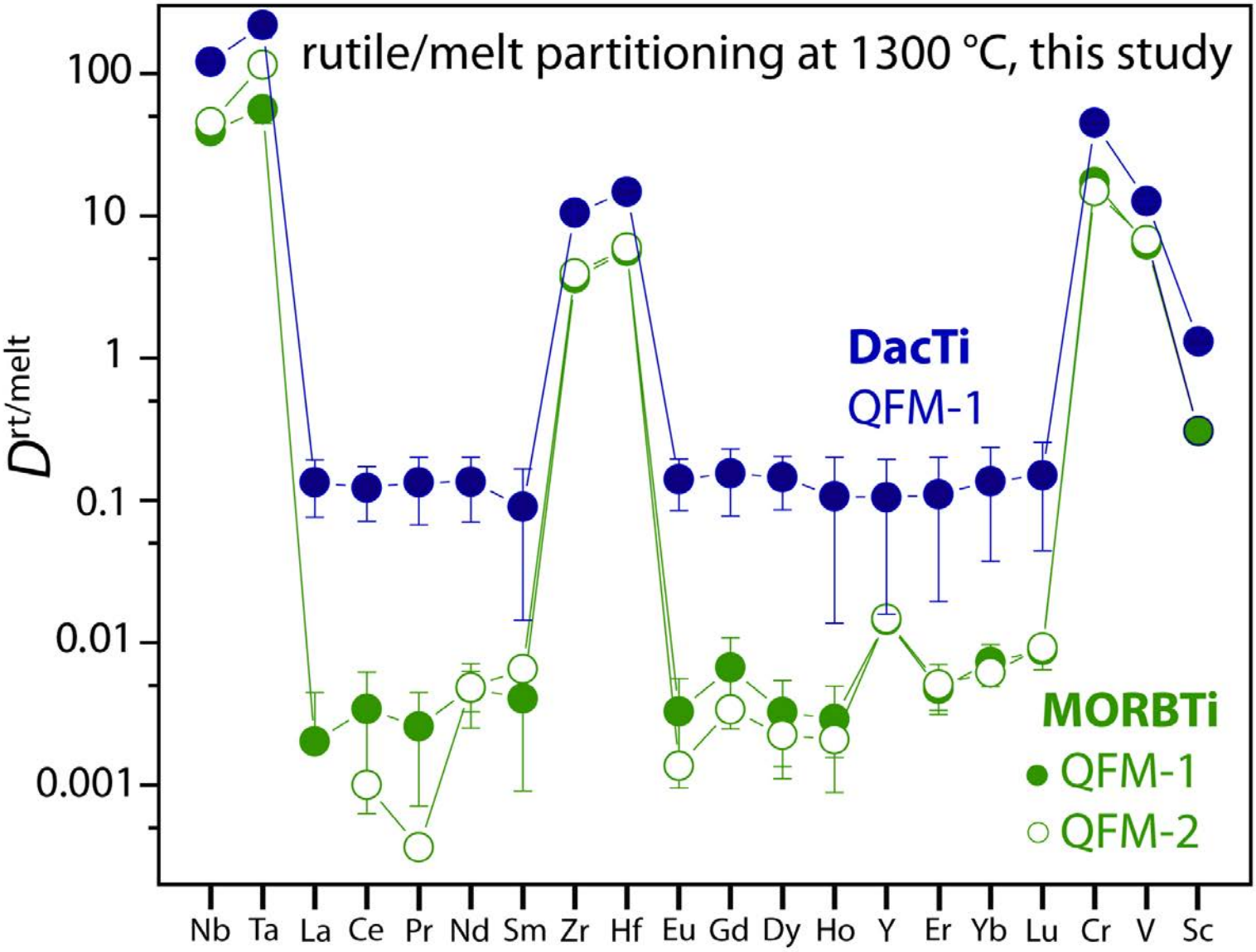

This is a preprint, the final version is subject to change, of the American Mineralogist (MSA)
Cite as Authors (Year) Title. American Mineralogist, in press.
DOI: https://doi.org/10.2138/am-2020-7013

Figure 8